JOURNAL OF GEOPHYSICAL RESEARCH, VOL. 105, NO. B11, PAGES 25,769–25,790, NOVEMBER 10, 2000

Segmentation in gravity and magnetic anomalies along the U.S. East Coast passive margin: Implications for incipient structure of the oceanic lithosphere

Mark D. Behn

MIT-WHOI Joint Program, Cambridge, Massachusetts

Jian Lin

Department of Geology and Geophysics, Woods Hole Oceanographic Institution, Woods Hole, Massachusetts

Abstract. Segmentation is a characteristic feature of seafloor spreading along the global mid-ocean ridge system. While segmentation of active spreading centers has been the focus of much recent research, the process by which a rifted continental margin develops into a segmented mid-ocean ridge is still poorly understood. In this study we investigate the segmentation character of the U.S. East Coast margin through a modeling study of the margin basement structure, magnetics, and gravity anomalies. The East Coast margin is of particular interest because it is one of several rifted continental margins that display thick sequences of high seismic velocity igneous crust, presumably formed during rifting. The East Coast Magnetic Anomaly (ECMA), a distinct total field magnetic high running offshore along the margin, is commonly located seaward of the thickest sections of the high-velocity crust and displays segmentation on length scales (100–120 km) similar to the segmentation observed at the Mid-Atlantic Ridge (MAR). Isostatic gravity anomalies were calculated by removing from free-air gravity the predicted effects of seafloor, sediments, and a crust-mantle model assuming local isostatic compensation. The resultant residuals show a corridor of high anomaly running along the margin, situated close to the maximum thickness of the high seismic velocity crust as determined from the two available seismic refraction lines. Reduction to the pole (R-T-P) of the total field magnetic anomaly shows that after the removal of skewness from the ECMA, the location of the isostatic gravity high is closely correlated to the ECMA. The isostatic gravity high is also segmented but in two distinct wave bands: 100–150 km and 300–500 km. The short-wavelength (100–150 km) segmentation in the R-T-P magnetic and isostatic gravity anomalies is similar in wavelength to segmentation in magnetization and mantle Bouguer anomaly observed along the present-day MAR. The 300–500 km segmentation in the along-margin isostatic gravity anomaly is similar in length scale to both intermediate-wavelength tectonic segmentation observed in the South Atlantic and variations in lithospheric strength observed along the African margin. Furthermore, two of the intermediate-wavelength (300–500 km) isostatic gravity lows correspond to the early traces of the Kane and Atlantis fracture zones, suggesting that these two fracture zones may define boundaries of a single tectonic corridor in the North Atlantic. We hypothesize that the direct cause of the intermediate-wavelength segmentation may be along-margin variations in both the amount of underplated igneous crust and the strength of the lithosphere, although the relative importance of these two effects remains unresolved. Our results imply that segmentation is an important feature of margin development and that segmentation at mature oceanic spreading centers may be directly linked to segmentation during continental rifting.

1. Introduction

Passive or rifted-continental margins result from the rifting of continents during the formation of a new ocean basin. Rifted margins are often classified as either volcanic or nonvolcanic on the basis of the amount of volcanism that occurs during rifting [e.g., *White and McKenzie*, 1989]. Volcanic margins are characterized by thick sequences of high seismic velocity (7.2–7.5 km/s) lower crust rocks (often referred to as underplating) and seaward dipping reflectors formed by the eruption and subsequent subsidence of volcanic flows during rifting. In contrast, nonvolcanic margins are generally associated with large rotated fault blocks, exposures of lower crustal and upper mantle rocks, and adjacent oceanic crust that is thinner than normal (3–4 km). Examples of volcanic margins include the Vøring Plateau [*Mutter et al.*, 1984], Hatton Bank [*White et al.*, 1987], and the Cuvier Margin [*Hopper et al.*, 1992], while nonvolcanic margins have been observed off Iberia [*Horsefield et al.*, 1993; *Whitmarsh et al.*, 1998] and along the Exmouth Plateau [*Hopper et al.*, 1992].

Early modeling efforts characterized rifting as a combination of stretching and thermal subsidence [e.g.,

Paper number 2000JB900292.
0148-0227/00/2000JB900292$09.00

McKenzie, 1978]. Although these models are capable of describing nonvolcanic margins, they are unable to account for the large sequences of igneous material found at volcanic margins. In an attempt to explain underplating, more recent models have focused on two principal mechanisms to form the high-velocity lower crust observed at volcanic margins: plume heads and secondary convection cells. Plume models require a thermal or chemical plume to be situated beneath the rifting crust [*White and McKenzie*, 1989]. The elevated mantle temperatures or chemical nature of the plume are hypothesized to cause enhanced decompression melting, leading to increased amounts of volcanism during passive rifting. Alternatively, *Mutter et al.* [1988] proposed that lateral temperature gradients, caused by the juxtaposition of hot upwelling mantle and cold continental crust during rifting, lead to the formation of secondary convection cells. These convection cells are hypothesized to generate active upwelling, which transports larger volumes of melt to the surface than would be allowed in a simple passive upwelling scenario [e.g., *Boutilier and Keen*, 1999].

Continental rifting is typically followed by the development of seafloor spreading along a margin. Spreading concentrates magmatic activity at a narrow ridge axis, which becomes the source of new oceanic crust. Mid-ocean ridge systems at slow spreading rates are documented to be highly three-dimensional in nature, with segmentation observed both at active spreading centers and in aged oceanic crust by the presence of fracture zones and off-axis traces of nontransform offsets [*Grindlay et al.*, 1991; *Sempéré et al.*, 1993; *Tucholke and Lin*, 1994] (see Figure 1). One topic of considerable research in recent years has been the relationship between segmentation and magma supply at the axis of a mid-ocean ridge. *Whitehead et al.* [1984] proposed that segmentation may be caused by gravitational instabilities that focus melt or mantle upwelling beneath spreading centers. This hypothesis has been supported by observations at slow spreading ridges, such as the Mid-Atlantic Ridge (MAR), where mantle Bouguer anomaly (MBA) lows are found at center of individual ridge segments [e.g., *Kuo and Forsyth*, 1988; *Lin et al.*, 1990; *Detrick et al.*, 1995]. These MBA "bull's-eye" patterns have been interpreted to represent focused mantle upwelling, which result in increased crustal thickness at the center of ridge segments and thinner crust toward the segment ends [*Kuo and Forsyth*, 1988; *Lin et al.*, 1990; *Lin and Phipps Morgan*, 1992]. On the other hand, magma supply at fast spreading ridges, such as the East Pacific Rise (EPR), appears to be more two-dimensional in nature with passive upwelling representing the major source of magma supply to the ridge-axis [*Parmentier and Phipps Morgan*, 1990; *Lin and Phipps Morgan*, 1992]. Alternatively, *Magde and Sparks* [1997] have recently suggested that crustal thickness variations along ridge segments may be caused by melt migration, as opposed to focused mantle upwellings. However, while many studies have examined magma supply at present-day ridges, few recent studies have addressed the possibility of segmentation in the supply of igneous underplated material to a continental margin preceding and during the initiation of seafloor spreading.

Studies in the Red Sea and West Africa suggest that passive margins may also exhibit three-dimensional structure. *Cochran and Martinez* [1988], for example, observed segmentation in both the marginal areas and axial valley of the Red Sea rift basin. In the Red Sea, "accommodation zones," or narrow regions that take up displacement between sets of fault blocks, extend perpendicularly across the passive margin and axial valley with an average spacing of 50-70 km. Intrusions of basaltic magma are observed in the axial valley at the centers of the segments defined by these accommodation zones. *Cochran and Martinez* [1988] interpreted these observations to indicate that segmentation has been present in the Red Sea rift since its inception. In addition, intermediate-wavelength segmentation has been observed along the continental margin offshore of West Africa. Using gravity anomalies, *Watts and Stewart* [1998] showed a 350–400 km long weak zone extending along the Gabon margin of western Africa, and hypothesized that the entire West African margin may exhibit segmentation of this scale with alternating segments of strong and weak lithosphere. However, while these studies suggest segmentation in margin structure, they do not examine the relationship between igneous underplating and margin segmentation.

In this study we investigate the segmentation character of the U.S. East Coast margin, interpreted to be a strongly volcanic margin, through a modeling study of the basement

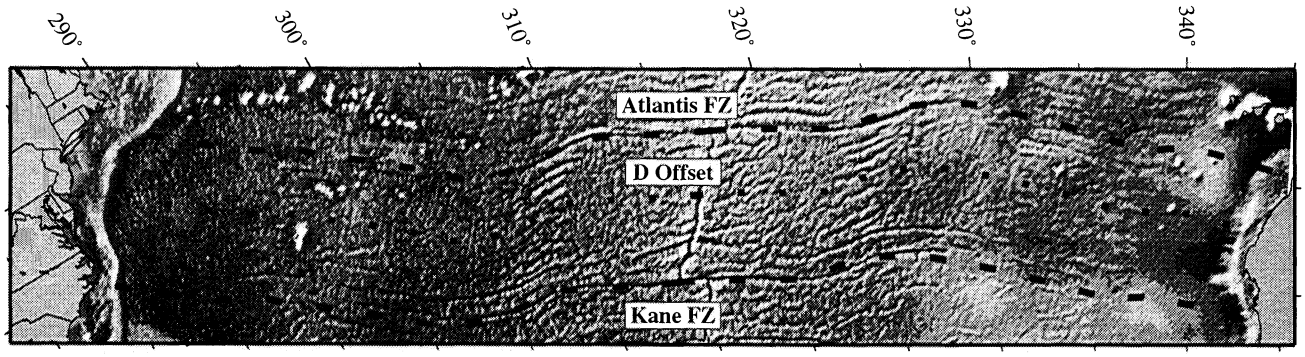

Figure 1. Free-air gravity of *Sandwell and Smith* [1997] illustrating the traces (dashed lines) of the Kane and Atlantis fracture zones from the U.S. East Coast margin to the conjugate West African margin. Also shown is a flow line (dotted line) projected from the intermediate-wavelength isostatic gravity low found near offset zone D between the Kane and Atlantis fracture zones.

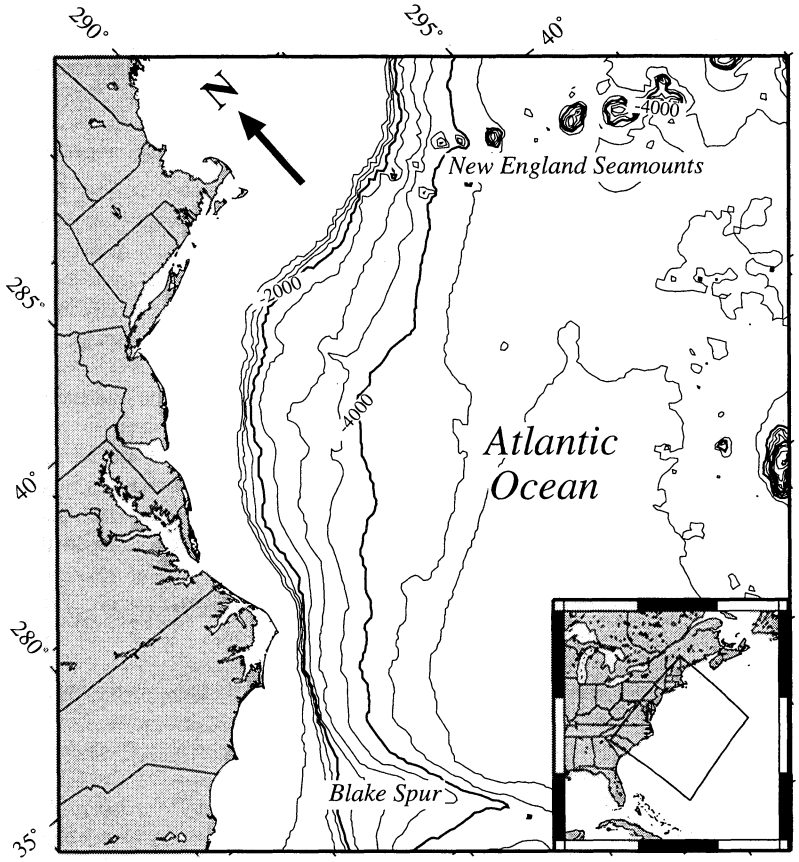

Figure 2. Location of the U.S. East Coast margin with bathymetry contoured at 500-m intervals. Inset shows an enlarged map of the U.S. East Coast used in Plate 1.

structure, magnetics, and gravity anomalies. We find that the magnetic and isostatic gravity anomalies are segmented along the margin strike at various wavelengths. On the basis of modeling of these anomalies and comparisons with previous seismic studies we propose that the same source may be responsible for both the magnetic and gravity anomalies along the margin. Finally, we show that the segmentation of these anomalies is generally correlated with the location of early traces of identifiable Atlantic offsets. In particular, the observed short-wavelength (100–150 km) segmentation is comparable to the spacing of major nontransform offsets at the present-day MAR, while the anomaly lows in the intermediate-wavelength (300–500 km) segmentation correspond to the incipient location of the Kane, Atlantis, and D offset zones (see Figure 1).

2. Geologic Setting

The U.S. East Coast margin (see Figure 2) was formed during the rifting of Pangea in the Late Triassic and Early Jurassic [*Klitgord et al.*, 1988]. *Klitgord and Schouten* [1986] suggested that seafloor spreading began around 175 Ma and has continued through the present. *Klitgord et al.* [1988] defined three across-margin structural zones landward to seaward across the East Coast margin: thinned continental crust, rift stage or transitional crust, and oceanic crust. Within the rift stage crust, subsidence has led to the formation of a number of large Mesozoic-Cenozoic sedimentary basins, such as the Carolina Trough, Baltimore Canyon Trough, Blake Plateau Basin, and Georges Bank Basin.

Three distinct magnetic anomalies are observed running parallel to the East Coast margin: the Brunswick Magnetic Anomaly (BMA), the East Coast Magnetic Anomaly (ECMA), and the Blake Spur Magnetic Anomaly (BSMA). The BMA is the landwardmost of the three magnetic anomalies, extending north from Georgia to Cape Hatteras, where it intersects the ECMA. The offshore portion of the BMA marks the hinge zone along the landward edge of the marginal sedimentary basins [*Klitgord et al.*, 1988]. The ECMA is a distinct magnetic high running parallel to the margin from the Blake Spur fracture zone (FZ) to Nova Scotia and is often taken to mark the continent-ocean boundary. Hypothesized sources for the ECMA include a highly magnetized ridge or intrabasement dike [*Klitgord and Behrendt*, 1979], faulting associated with rifting [*Alsop and Talwani*, 1984], an edge effect between transitional and oceanic crust [*Hutchinson et al.*, 1983], and rift-related volcanics [*Austin et al.*, 1990]. However, recent magnetics modeling of across-margin seismic refraction profiles strongly support the last mechanism as the source of the ECMA [*Austin et al.*, 1990; *Talwani et al.*, 1995]. The BSMA is the seawardmost of the three magnetic anomalies and has been associated with a ridge jump around 170 Ma [*Klitgord and Schouten*, 1986].

Over the last 2 decades a number of studies have focused on the volcanic character of the U.S. East Coast margin. Studies in the mid-1980s first suggested that the East Coast margin might be characterized by significant amounts of igneous underplating. *Hinz* [1981] and *Klitgord et al.* [1988] interpreted seaward dipping reflectors in multichannel seismic data from the Baltimore Canyon Trough and offshore of Georges Bank, respectively, as evidence for volcanism associated with rifting. Moreover, wide-angle seismic lines across the Baltimore Canyon Trough [*LASE Study Group*, 1986] and the Carolina Trough [*Tréhu et al.*, 1989a] have found high lower crustal velocities (7.2–7.5 km/s) beneath the transitional crust. Additional analyses of multichannel and wide-angle seismic data by *Holbrook et al.* [1994a, 1994b] across the Carolina Trough and offshore of Virginia show ~25 km thick sequences of high-velocity lower crust, interpreted as large intrusions of underplated igneous material. On the basis of these studies, *Holbrook and Kelemen* [1993] concluded that the U.S. East Coast margin is characterized by a 20–25 km thick section of high-velocity igneous material, emplaced at rifting and extending over 1000 km along the margin.

Invoking a plume model, *White and McKenzie* [1989] hypothesized that the Cape Verde hot spot, situated near the center of the East Coast margin, generated a broad (~1000 km) thermal anomaly in the asthenosphere capable of producing the observed sequences of high-velocity material. *Kelemen and Holbrook* [1995] pointed out that a thermal anomaly centered on the Cape Verde hot spot should have generated a radially symmetrical pattern of igneous underplating, and yet no such systematic changes in the amount of underplating have been observed from seismic studies along the East Coast [*Holbrook and Kelemen*, 1993]. Therefore, as an alternative to the plume model, *Kelemen and Holbrook* [1995] proposed that the thick sequences of igneous crust were formed by a short-lived thermal anomaly in the upper mantle running along the entire margin, which dissipated rapidly after the initiation of normal seafloor spreading.

3. Data Sources

The goal of this study is to obtain a better understanding of the dynamics of magmatism during rifting along the U.S. East Coast through an analysis and joint interpretation of magnetic and isostatic gravity anomalies. In particular, we are interested in correlations between these two independent data sets that may provide new insights into the three-dimensional nature of magmatism during rifting and the incipient structure of the oceanic lithosphere. The main types of data used in this study are addressed briefly in this section.

3.1. Magnetic Field

The magnetic field data used in this study were obtained from the Geological Survey of Canada (GSC) [*Verhoef et al.*, 1996], providing 5 km spatial coverage across the U.S. East Coast margin (Plate 1). This data set consists of a compilation of shipboard magnetic surveys, aeromagnetic data, and previously gridded data sets from the period 1956–1992. These data have been correctly referenced to the International Geomagnetic Reference Field (IGRF) and filtered to remove anomalies with wavelengths >400 km. The final gridded data set represents the total field magnetic anomaly across the East Coast margin and clearly illustrates the ECMA running parallel to the margin and the high magnetic anomalies associated with the New England Seamounts (Plate 1).

3.2. Bathymetry and Sediment Thickness

In order to accurately correct for topographic effects in the free-air gravity, bathymetry of as high quality as possible is desired. The bathymetry data used in this study consist of ship track data obtained from the National Geophysical Data Center supplemented with ETOPO5 digital data between ship tracks. In order to give a greater weight to the higher quality ship track data, all ETOPO5 data points within 5 min of a shiptrack were eliminated and the combined data set was then regridded on a 3 min grid to produce the bathymetry map shown in Figure 2 and Plate 2a. The bathymetry map clearly illustrates the three major physiographic features of the East Coast margin: the continental shelf, continental slope, and continental rise. Also shown in the bathymetry are the New England Seamount Chain located southeast of Cape Code, Massachusetts [*Uchupi et al.*, 1970], and the Blake Plateau and Ridge located offshore of South Carolina [*Dillon and Popenoe*, 1988].

In addition to bathymetry, sediment thickness data were also acquired for the East Coast margin. The sediment thickness data shown in Plate 2a were extracted from 5 min digital sediment grids of the U.S. Geological Survey (USGS) [*Klitgord et al.*, 1994; *Hutchinson et al.*, 1996] and then resampled onto a 3 min grid. The USGS sediment thickness data are based on seismic reflection profiles, which have been verified against seismic refraction data and stratigraphic test wells where available. The USGS data are supplemented with data from *Tucholke et al.* [1982] in the region between 290°E and 295°E. Sediment thickness is highly variable across the margin, reaching a maximum thickness of 12–14 km within the marginal sedimentary basins. Thus, in order to correct the gravity data for the effects of the low-density sediment layers, it is essential to have an accurate estimate of sediment thickness across the margin, such as the one available here along the U.S. East Coast.

3.3. Free-Air Gravity

The free-air gravity map shown in Plate 2b was extracted from the 2 min satellite gravity map of *Sandwell and Smith* [1997]. A prominent high-low couple in the free-air gravity is situated over the transition between the continental shelf and slope, extending along the length of the margin. This feature, often referred to as the "continental edge effect," results from the abrupt transition from thick continental crust to thin oceanic crust. *Watts and Marr* [1995] have used this edge effect to characterize the strength of continental margins, showing that mechanically strong margins generally have a single high-low couple, while mechanically weak margins are often characterized by two high-low couples of smaller amplitude.

3.4. Uncertainties in Offset Zone Locations

In order to characterize the nature of segmentation in the lithosphere adjacent to the East Coast margin, we used offsets in the magnetic field data to identify the major offset zones present during the Jurassic period. Previous studies [e.g., *Klitgord and Schouten*, 1986] calculated average stage poles

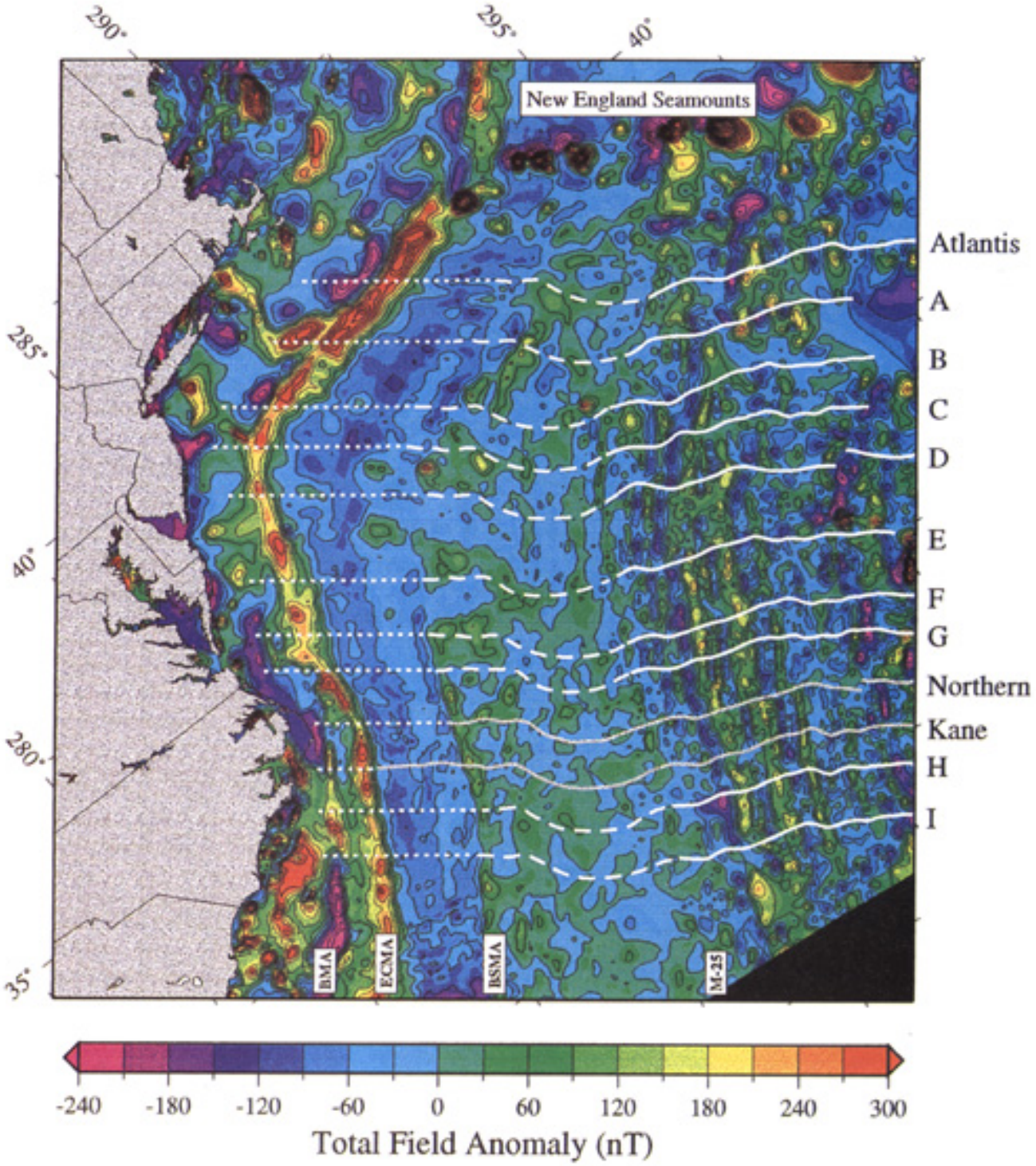

Plate 1. Total field magnetic anomaly from the Geological Survey of Canada [*Verhoef et al.*, 1996]. Areas without adequate data control are masked in black. The segmented magnetic high running parallel to the margin is the East Coast Magnetic Anomaly (ECMA). Solid gray lines show the location of the Kane and Northern fracture zones as mapped by *Tucholke and Schouten* [1988] on the basis of a combination of basement structure and magnetic data. White lines illustrate the location of the offset zone traces identified in this study. Solid lines represent areas where the offset zone traces are constrained by offsets in magnetic lineations; dashed lines are used where the traces are primarily constrained from the flow lines of *Tucholke and Schouten* [1988]. The dotted lines are used to represent the high uncertainty in the location of the offset zone traces between the BSMA and the margin. Labels identifying the major offset zones (Atlantis, Kane, Northern, and A–I) are located in the right-hand margin.

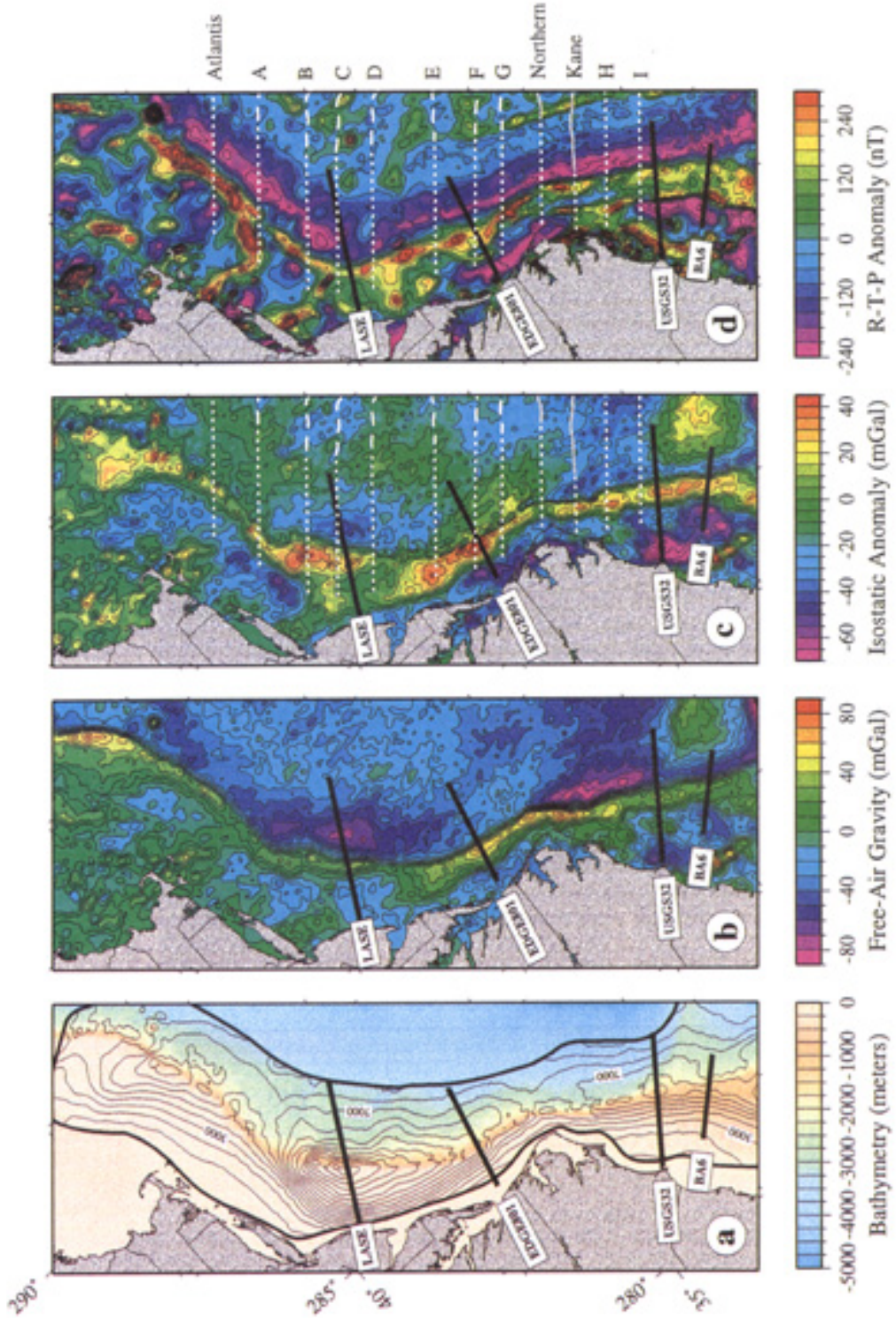

Plate 2. (a) Shaded bathymetry of the U.S. East Coast, combining National Geophysical Data Center (NGDC) ship track data and ETOPO5 digital bathymetry data. In areas where NGDC ship tracks were located within 5 min of a grid point the NGDC data were used; in all other areas ETOPO5 data were used. Light black contour lines show sediment thickness from USGS seismic reflection grids, while thick black lines illustrate the extent of the USGS data coverage. (b) Free-air gravity derived from *Sandwell and Smith's* [1997] satellite gravity map. (c) Isostatic gravity anomaly, calculated by subtracting from the free-air gravity the effects of the water-sediment ($\Delta\rho$ = 1300 kg/m^3), sediment-crust ($\Delta\rho$ = 400 kg/m^3), and crust-mantle ($\Delta\rho$ = 600 kg/m^3) interfaces. The depth to the crust-mantle interface was calculated from the bathymetry and sediment thickness data assuming local Airy isostasy. See Plate 1 for notation on offset zone traces. (d) Reduced-to-the-pole (R-T-P) magnetic anomaly along the East Coast margin.

for the North American plate by examining seafloor magnetic lineations during periods of major changes in plate motion. However, the flow lines calculated from these stage poles and projected back from major offset zones at the present-day MAR axis represent only the average offset zone traces with time. It has been shown that small offset discontinuities are subject to migration along a plate boundary [e.g., *Grindlay et al.*, 1991; *Tucholke et al.*, 1997] and that the offset length of a fracture zone can vary from near zero to over 150 km over its life span (e.g., the Kane FZ [*Tucholke and Schouten*, 1988]). Thus it is possible that fracture zones and nontransform offsets that display significant offset length today may have had much smaller offsets and experienced along-axis migration at some point in the past. For this reason we deemed it necessary to reassess the location of Jurassic offset zones using the high quality GSC magnetic field data.

The major offset zones shown in Plate 1 were picked on the basis of offsets in seafloor magnetic lineations from the reduced-to-the-pole GSC data (see also section 4.2). To insure that our identification of the major offsets was consistent with the known North American plate motion for the Jurassic, we used the location of the Kane and Northern fracture zones as determined by *Tucholke and Schouten* [1988] as a guide. *Tucholke and Schouten* [1988] used a combination of basement topography and magnetic anomalies to map the Kane and Northern fracture zone traces. More recent work along the conjugate West African margin by *Verhoef et al.* [1991] and *Roest et al.* [1992] further support the flow line picks of *Tucholke and Schouten* [1988], and thus we believe that their study provides the best available flow line constraint for the western North Atlantic.

Well-developed magnetic lineations are observed in the oceanic crust eastward of anomaly M-25 (see Plate 1). However, few clear lineations can be seen in crust formed during the Jurassic magnetic quiet zone [*Vogt*, 1973] between anomaly M-25 and the BSMA. This contrast in the amplitude of the observed magnetic lineations leads to less certainty in our identification of the offset zone traces in the region between M-25 and BSMA, where our picks are heavily dependent on flow lines of *Tucholke and Schouten* [1988]. West of the BSMA, there is even less constraint on the location of the offset zone traces. Using the limited amount of magnetic and seismic data available at the time, *Klitgord and Schouten* [1986] and *Tucholke and Schouten* [1988] observed the offset zone traces to trend approximately northwest across the BSMA until they intersect the ECMA. Thus, the highest uncertainty is assigned to the offset zone traces in the region between the BSMA and ECMA.

4. Gravity and Magnetic Anomalies

The free-air gravity signal comprises a number of effects, including those from seafloor topography, sediments, and the crust-mantle interface. In order to isolate local anomalies in the crust and mantle, we used the method described by *Parker* [1972] to extract the theoretical effects of the water-sediment ($\Delta\rho$ = 1300 kg/m^3), sediment-crust ($\Delta\rho$ = 400 kg/m^3), and crust-mantle ($\Delta\rho$ = 600 kg/m^3) interfaces. In areas of relatively little sedimentation and uniform oceanic crust, such as at mid-ocean ridges, a reference model of constant crustal thickness is often used, against which mantle Bouguer anomalies are calculated by removing the effects of a reference model of uniform crustal thickness and density [*Kuo and Forsyth*, 1988; *Lin et al.*, 1990]. However, in a margin setting, where the lateral change in crustal thickness from continental to oceanic crust can be up to a few tens of kilometers, a reference model of constant crustal thickness is no longer a good option [see *Simpson et al.*, 1986]. Therefore, for the U.S. East Coast margin we calculated isostatic gravity anomalies against a reference model in which local Airy isostasy is assumed for the crustal column. The resultant isostatic gravity anomaly is shown in Plate 2c. We note that while using slightly different density parameters makes subtle changes to the detailed shape and magnitude of the isostatic anomaly, it does not alter the overall pattern of anomalies shown in Plate 2c. The isostatic anomaly calculated here compares well to that of *Simpson et al.* [1986], who calculated regional isostatic gravity anomalies for the continental United States. The largest discrepancies between the two studies are found in the regions where the sediment thickness is greatest (e.g., Baltimore Canyon Trough), illustrating the importance of incorporating the USGS sediment thickness data, which was unavailable to the study of *Simpson et al.* [1986].

4.1. Comparison to Across Margin Seismic Lines

Seismic studies represent the best tool currently available for imaging crustal structure. However, seismic transects are often limited to very few profiles across the area of interest. On the other hand, while gravity and magnetic maps are useful for revealing regional-scale lateral variations in anomalies, the interpretation of these anomalies is inherently nonunique. Therefore, in an attempt to better understand the implications of the observed geophysical anomalies along the U.S. East Coast margin, we examine in detail the isostatic gravity and magnetic anomalies along the two most recently available high-resolution seismic transects: EDGE-801 [*Holbrook et al.*, 1994a] and BA-6 [*Holbrook et al.*, 1994b] (Figures 3 and 4, respectively) as well as the Large Aperture Seismic Experiment (LASE) [*LASE Study Group*, 1986] and the USGS32 [*Klitgord et al.*, 1988; *Tréhu et al.*, 1989a] seismic lines (Figure 5).

Along the four seismic transects examined, it appears that the peak in the isostatic gravity anomaly is situated directly over the region of high velocities in the lower crust (see Figures 3, 4, and 5). On the other hand, the position of the total field of the ECMA appears to be shifted seaward of the underplated material along the EDGE-801, BA-6, and USGS32. This seaward shift in the total field of the ECMA was observed by *Holbrook and Kelemen* [1993], who found the total field magnetics peak to be located between the thickest portion of the seaward dipping wedge and the landward limit of the oceanic crust. *Holbrook et al.* [1994a] and *Talwani et al.* [1995] have modeled the spatial correlation between the total field magnetics and high seismic velocities and suggested that the igneous rocks emplaced during rifting may act as the source for the ECMA.

Along the LASE line (Figures 5a and 5b), the relationship between the peak of the isostatic gravity anomaly and the total field of the ECMA is reversed from the other three seismic lines, with the isostatic gravity high located slightly seaward of the ECMA. One potential explanation for this seaward shift in the isostatic gravity high is related to the high-density carbonate reef identified between 120 and 160 km on the LASE line [*Tréhu et al.*, 1989b]. Furthermore, the

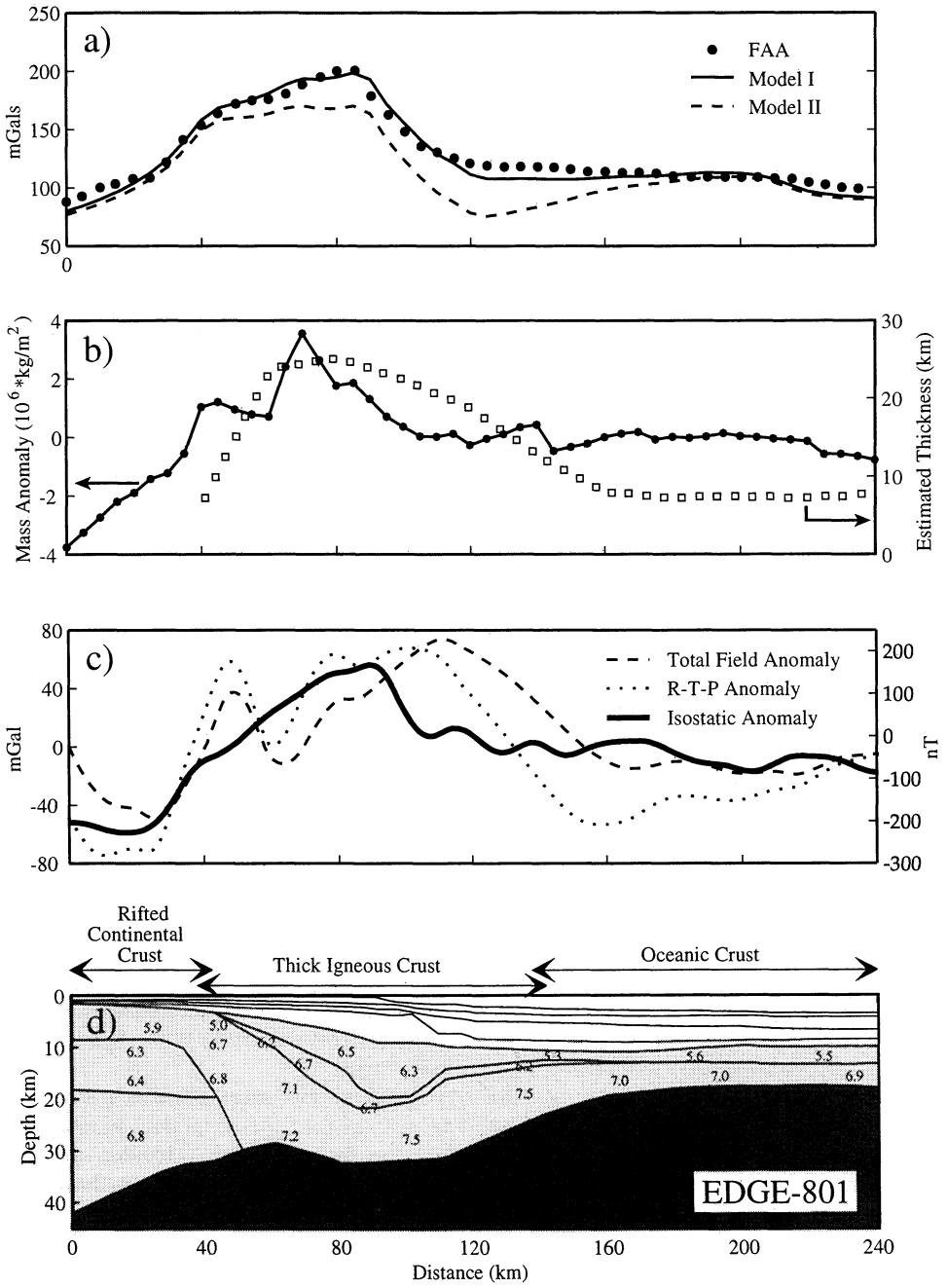

Figure 3. Comparison of the EDGE-801 seismic line [*Holbrook et al.*, 1994a] to observed geophysical anomalies. (a) Observed free-air gravity (FAA) (solid circles) versus modeled gravity. Model I is based on the density structure of *Holbrook et al.* [1994a], while model II uses a reduced lower crustal density of 3030 kg/m^3. Note that without the crustal density structure of *Holbrook et al.* [1994a] it would be difficult to reproduce the observed free-air gravity without assigning unreasonable densities to the upper crust. (b) Mass anomaly (solid circles) that results from the density structure of *Holbrook et al.* [1994a]. The relative mass anomaly is calculated by integrating the mass with depth in individual columns along the seismic profile and comparing to a reference model for normal oceanic crust. Open squares represent the estimated thickness of emplaced igneous rocks by *Holbrook and Kelemen* [1993]. (c) Isostatic gravity, total field magnetic, and reduced-to-pole (R-T-P) magnetic anomalies sampled along the profile. (d) Crustal velocity model along the EDGE-801 line adapted from *Holbrook et al.* [1994a]. Note the good correlation between the isostatic mass anomaly in Figure 3b and the calculated isostatic gravity anomaly and R-T-P magnetic anomaly in Figure 3c. Moreover, the maximum isostatic anomaly appears to be located directly over the region of thick, high-velocity lower crust.

high-velocity lower crust along the LASE line appears to be broader in horizontal extent than along the three other seismic lines.

We carried out simple forward models to illustrate the relationship between igneous crust of high seismic velocity in its underplated section and the resulting gravity and magnetic anomalies. Figure 6 shows the isostatic gravity anomaly and magnetic anomalies associated with a simplified crustal density model for an underplated margin. This model reveals an isostatic anomaly of 50–60 mGal situated directly over the region of high velocity and density in the lower crustal rocks. The total field magnetic anomaly was calculated in the manner of *Plouff* [1976] with a Curie depth of 20 km. Induced magnetization from the present-day field (inclination of 68°, declination of -13°, field strength of 50,000 nT) was assumed for the crustal block, while remanent magnetization in the direction of the Jurassic field (inclination of 46°, declination of -2.2° [*Austin et al.*, 1990]) was used for the seaward dipping reflector sequence situated above the underplated section. *Talwani et al.* [1995] argued convincingly that the ECMA must be generated by remanent magnetization of volcanic flows produced by subaerial seafloor spreading. They based their assumption on the very high remanent magnetization of volcanic rocks from Ocean

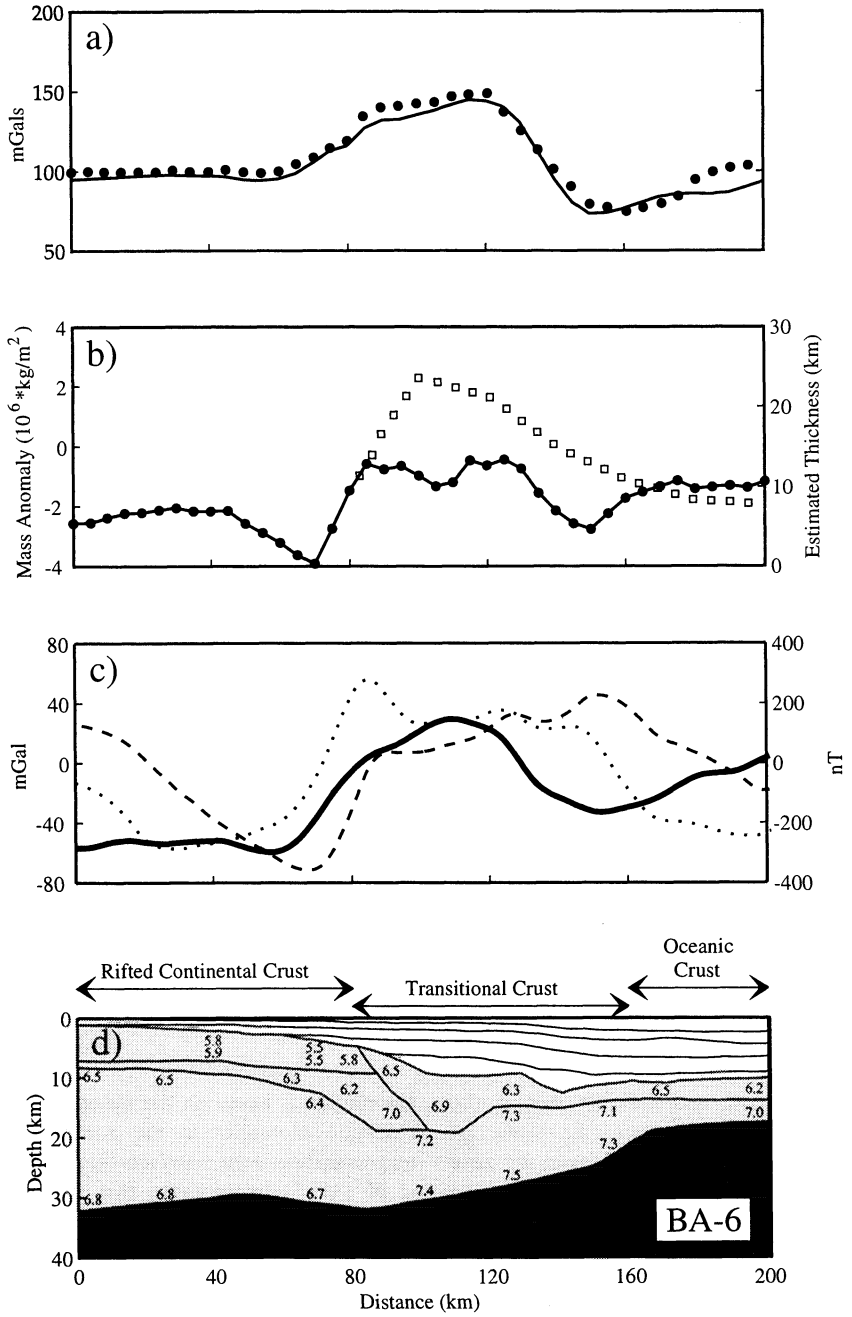

Figure 4. Comparison of the BA-6 seismic line [*Holbrook et al.*, 1994b] to observed geophysical anomalies. See Figure 3 for notation.

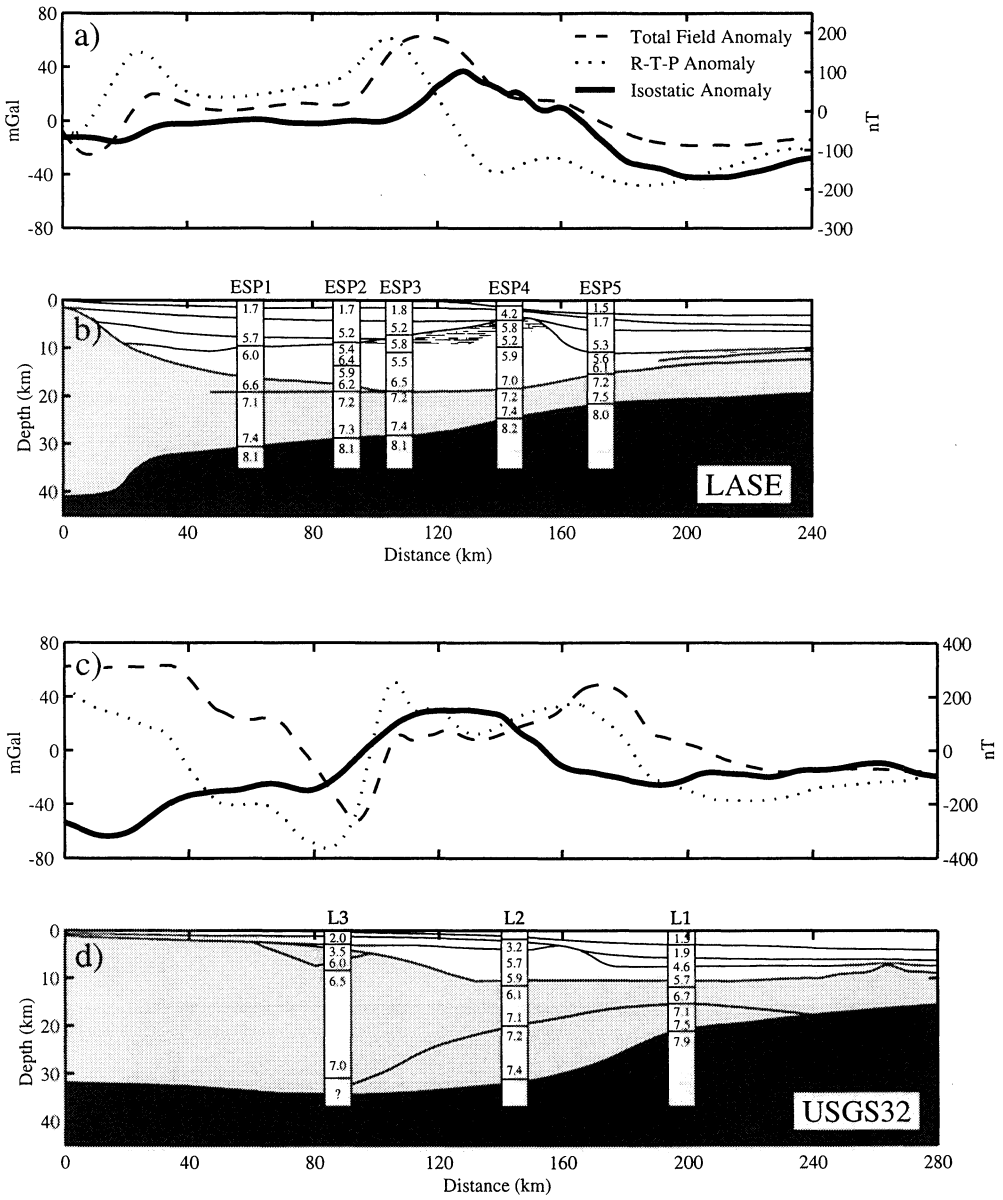

Figure 5. (a,b) Comparison of the LASE seismic line [*LASE Study Group,* 1986] to observed geophysical anomalies. Crustal velocities are constrained by five expanded spread profiles (ESPs) shown in Figure 5b. Note that along this profile the peak in the isostatic gravity anomaly lies seaward of the peak in the R-T-P anomaly and correlates closely with the location of the carbonate reef (patterned region) identified in the seismic profile. (c,d) Comparison of USGS32 seismic line [*Klitgord et al.*, 1988] to observed geophysical anomalies. Crustal velocities are determined from three large-offset seismic profiles oriented perpendicular to the USGS32 line [*Tréhu et al.,* 1989a] shown in Figure 5d.

Drilling Program (ODP) Hole 642, and the fact that if the ECMA were due to induced magnetization, the value of susceptibility would be unacceptably large. However, we note that given the similarity in inclination and declination of the present-day and Jurassic fields, modeling the seaward dipping reflector sequence with only an induced component would produce nearly identical anomalies to those produced by remanent magnetization.

Similar to the magnetic modeling of *Talwani et al.* [1995], we assume that oceanic crust seaward of the seaward dipping reflector sequence to have zero effective magnetization. This assumption is based on the observation of small amplitude of magnetic anomalies in the oceanic crust lying within the magnetic quiet zone between the ECMA and BSMA. *Talwani et al.* [1995] hypothesize that this magnetic quiet zone is most likely caused by the juxtaposition of normally and reversely polarized subhorizontal lava flows emplaced subaerially during a period of slow seafloor spreading. The magnetic model shown in Figure 6 illustrates that as observed in the EDGE-801, BA-6, and USGS32 seismic lines, the peak in the total field anomaly is shifted seaward of the underplated section. Thus both the isostatic gravity high and

total field magnetic high can be explained from the same sequence of high-density lower crustal rocks and corresponding seaward dipping reflectors in the upper crust associated with the formation of the East Coast margin.

In addition, it can be seen that the strike of the margin has a significant effect on the amplitude of the total field magnetic anomaly (Figure 6). We calculated two examples with strikes of 30° and 90° to represent the East Coast margin off North Carolina and Long Island, respectively. The calculated peak in the total field anomaly along the margin striking 90° is ~200 nT greater than the margin striking 30°. Hence the observed increase in amplitude of the total field ECMA offshore of Long Island may represent the change in the margin trend and not necessarily an increase in the strength of the magnetic source body. Alternatively, the increase in amplitude of the total field ECMA toward the northeastern extreme of the margin may be caused by the observed shallowing of the basement depth in this region (Figure 7). Figure 7a illustrates that burying the idealized margin shown in Figure 6 with 5 km of nonmagnetized sediments decreases the peak of the total field magnetic anomaly by ~50%. We note that the isostatic gravity anomalies should not be affected by these variations in sediment thickness since the sediment effects have been taken into account during the gravity calculations.

To further investigate the relationship between the isostatic gravity anomaly and the seismic data, we used the seismically derived density models of *Holbrook et al.* [1994a,

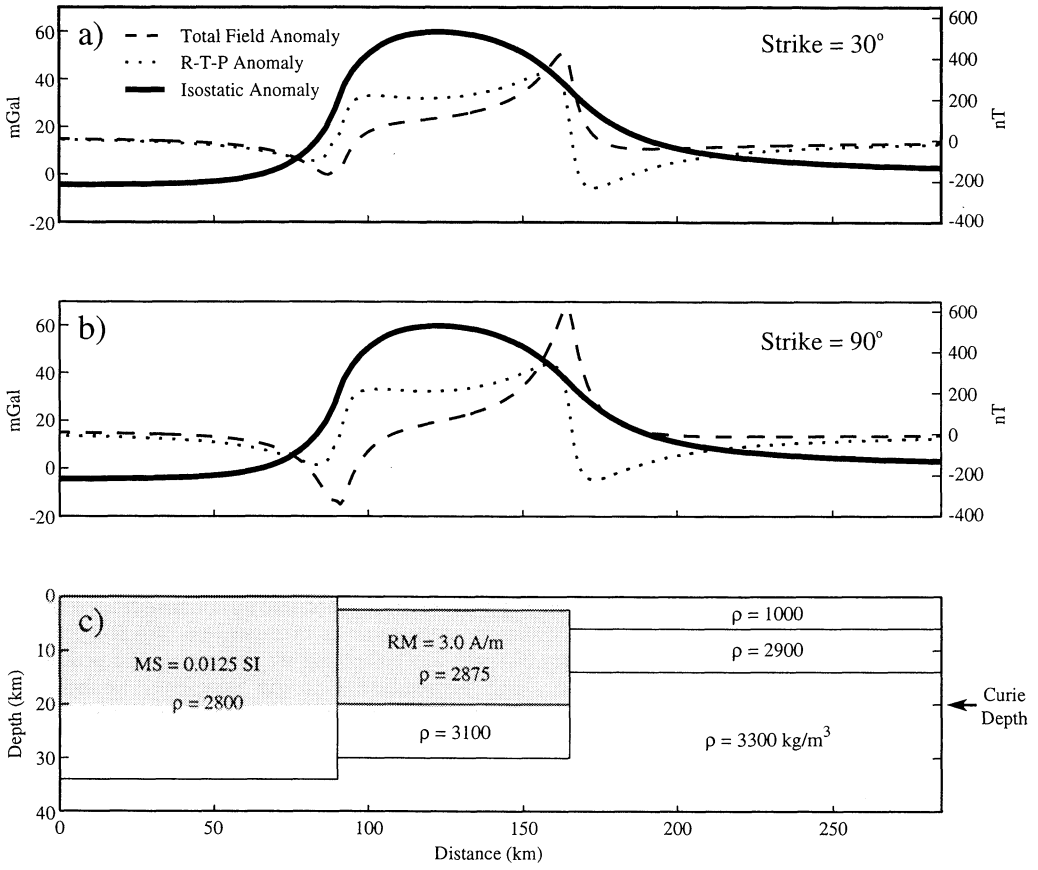

Figure 6. Illustration of gravity and magnetic anomalies produced by an idealized margin with underplated lower crust that is not in local isostatic equilibrium. (a) Isostatic gravity (solid line), total field magnetic (dashed line), and R-T-P magnetic (dotted line) anomalies produced from a margin striking 30°E of magnetic north corresponding to the margin offshore of North Carolina. (b) Anomalies produced from a margin striking 90°E of magnetic north corresponding to a location offshore of Long Island, New York. (c) Block model illustrating the densities and magnetizations used for the models shown in Figures 6a and 6b. Induced magnetization is assumed for the continental block with magnetic susceptibility (MS) of 0.0125 SI, while a remnant magnetization (RM) of 3.0 A/m is used for the seaward dipping reflector sequence. The strength of the present-day magnetic field is taken to be 50,000 nT with an inclination of 68° and a declination of -13°. We assumed an Early Jurassic paleofield for the remnant magnetization (inclination of 46°, declination of -2.2° [*Austin et al.*,1990]) and a Curie depth of 20 km for both models. The shift in the peak of the total field magnetic anomaly ~50 km seaward of isostatic gravity high is similar to the observed seaward offset of the ECMA total field along the EDGE-801, BA-6, and USGS32 seismic lines. Density values of 2875 and 3100 kg/m^3 were assumed for the upper seaward dipping reflector block and lower high seismic velocity block, respectively. Densities were 2800 kg/m^3 for the continental crust block and 2900 kg/m^3 for the oceanic crust.

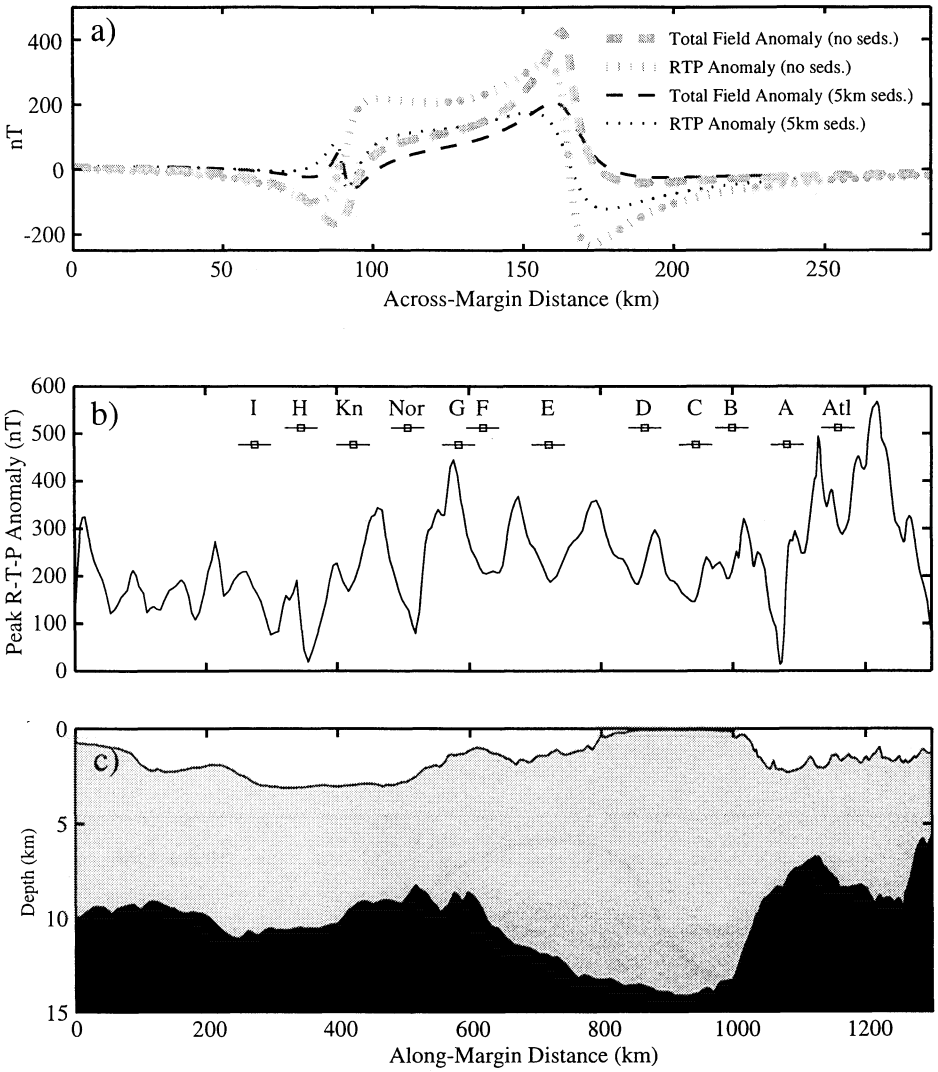

Figure 7. (a) Comparison of total field and R-T-P magnetic anomalies generated by a nonsedimented margin and a margin buried with 5 km of sediment. Model geometry is the same as in Figure 6c. (b) R-T-P magnetic anomaly along the peak of the ECMA. Along-margin distance was calculated by projecting the profile in the average flow line direction and then taking the distance perpendicular to the flow lines as the standard distance. (c) Along-margin profile of bathymetry and basement depth (water, sediment, and crust shown in white, shaded, and black, respectively). Notice that the R-T-P anomalies are greatest toward the northeastern extreme of the margin where the basement depths are shallowest.

1994b] to calculate the isostatic mass anomaly along each profile (Figures 3 and 4). The mass anomalies were calculated by integrating the mass with depth in individual columns along each seismic profile and compared with the total mass of an idealized crustal reference model. Figures 3b, 3c, 4b, and 4c show that there is a strong correlation between the isostatic mass anomaly as calculated from the density models of *Holbrook et al.* [1994a, 1994b] and the isostatic gravity anomaly. To address the concern that the strong observed correlation may reflect the use of gravity data in the density modeling by *Holbrook et al.* [1994a; 1994b], we also compared the isostatic gravity anomaly with the total estimated thickness of igneous rocks emplaced during rifting [*Holbrook and Kelemen*, 1993]. This method of analysis shows an excellent correlation between the isostatic gravity and the amount of material emplaced during rifting. Moreover, since the crustal thickness data have been interpreted directly from the seismic velocities, they contain no a priori dependence on the gravity signal. We conclude that the isostatic gravity anomaly is a useful indicator of variations in the amount of crustal volume along the margin.

On the basis of the cross-sectional area of the thickened igneous crust along the EDGE-801 and BA-6 seismic lines (see Figures 3b and 4b, respectively), *Holbrook and Kelemen* [1993] estimated the total volume of igneous material emplaced along the East Coast margin to be 3.2×10^6 km^3. However, Plate 2c shows that both the EDGE-801 and BA-6 lines cross the margin at locations of relatively high values of isostatic gravity anomaly. Thus extrapolating the amount of igneous crust emplaced along the margin from these two seismic profiles alone may overestimate the total volume of igneous material. To provide a better estimation, we

calculated a transfer function between the isostatic gravity anomaly and the thickness of igneous crust using the data from the EDGE-801 and BA-6 seismic lines (Figure 8a). Clearly, density variations throughout the crustal column independent of underplating may also affect the isostatic anomaly, potentially leading to much of the scatter observed in Figure 8a. However, the correlations shown along the EDGE-801 and BA-6 lines in Figure 8a strongly suggest that the isostatic anomaly is largely dependent on the amount of emplaced igneous crust, and thus the isostatic anomaly can be used as a proxy for examining variations in the underplating process along the margin.

We applied the transfer function of Figure 8a to a series of across-margin profiles of isostatic gravity anomaly (spaced 1 km apart along the margin) to determine the cross-sectional area of igneous material along each profile (Figure 8c). On the basis of the seismic profiles in Figures 3, 4, and 5 we estimated the maximum width of the magmatic emplacement zone to be ~200 km and applied our transfer function to a 200 km wide window centered on the peak of the isostatic anomaly. In order to estimate only the excess igneous material emplaced during rifting, we subtracted from this value the amount of igneous material due to a normal thickness (6 km) oceanic crust seaward of the peak in the

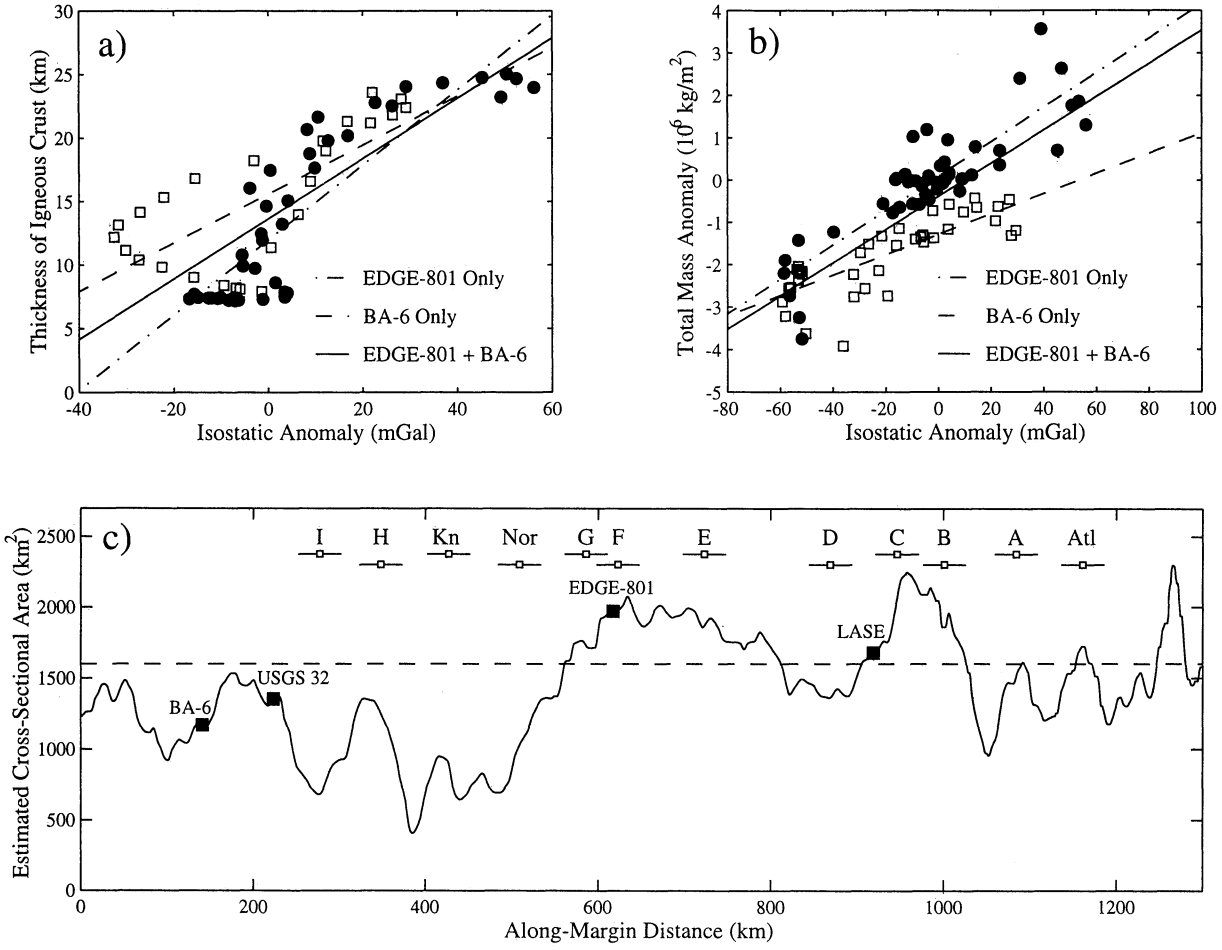

Figure 8. (a) Correlation between the isostatic gravity anomaly and the total thickness of igneous crust along the EDGE-801 (solid circles) and BA-6 (open squares) seismic lines. The transfer function calculated from the EDGE-801 data only (dash-dotted line) is $y = 12.0 + 0.30$ * isostatic anomaly ($r^2 = 0.76$); from the BA-6 data only (dashed line) is $y = 15.6 + 0.19$ * isostatic anomaly ($r^2 = 0.53$); and from both data sets combined (solid line) is $y = 13.7 + 0.24$ * isostatic anomaly ($r^2 = 0.61$). (b) Correlation between the isostatic gravity anomaly and the total mass anomaly along the EDGE-801 (solid circles) and BA-6 (open squares) seismic lines. The transfer function calculated from the EDGE-801 data only (dash-dotted line) is $y = 0.098 + 0.041$ * isostatic anomaly ($r^2 = 0.75$); from the BA-6 data only (dashed line) is $y = -1.28 + 0.024$ * isostatic anomaly ($r^2 = 0.64$); and from both data sets combined (solid line) is $y = -0.38 + 0.039$ * isostatic anomaly ($r^2 = 0.66$). (c) Along-margin variations in the estimated cross-sectional area of igneous material emplaced at individual across-margin profiles of isostatic gravity anomaly (spaced at 1 km apart along the margin). The estimation was based on the best fitting transfer function between the isostatic gravity anomaly and the total thickness of igneous crust using the combined data sets of the EDGE-801 and BA-6 seismic lines (solid line in Figure 8a). Dashed line illustrates the representative value of cross-sectional igneous material used by *Holbrook and Kelemen* [1993], which appears to overestimate the average values along the margin by ~12.5%. Solid squares show the locations of the four across-margin seismic lines identified in Plate 2.

isostatic anomaly. Using this method, we calculated the amount of igneous material emplaced at individual across-margin profiles to range from 410 to 2300 km^2 , with an average value of ~1400 km^2 for the whole margin. This average value is ~87.5% of the average value from the EDGE-801 (1800 km^2) and BA-6 (1400 km^2) obtained by *Holbrook and Kelemen* [1993], suggesting that they may have overestimated the total amount of igneous material emplaced along the East Coast margin by ~12.5%. Our method assumes that the entire isostatic anomaly can be attributed to variations in the underplating process. However, in certain areas, density variations in the crustal column independent of underplating may also contribute to the isostatic anomaly (e.g., the carbonate reef observed in the LASE line). Thus our calculation of the amount of emplaced igneous material should be viewed only as a qualitative estimate for variations along the margin.

4.2. Reduction-to-the-Pole Magnetic Anomalies

Although isostatic gravity anomalies are typically situated directly over their source mass, this may not be the case for total field magnetic anomalies (Figure 6). Variations in magnetization direction and the direction of the Earth's present-day field may cause the total field anomaly to be distorted in shape and shifted laterally in position relative to its source mass. To correct for this effect, we performed a two-dimensional reduction-to-the-pole (R-T-P) analysis on the total field magnetic anomalies using the method of *Blakely* [1995]. The resulting R-T-P anomalies represent the magnetic anomaly that would be generated if both the magnetization and ambient field were directed vertically. Therefore anomalies that have been reduced to the pole are situated over their respective source body and altered in shape such that a symmetrical source generates a symmetrical anomaly.

In order to perform the reduction-to-the-pole calculation it is necessary to assume an inclination and declination for both the present-day field and the remanent magnetization direction. The mean inclination and declination of the present-day field across the East Coast margin were calculated from the IGRF to be 68° and -13°, respectively. The Jurassic field of *Austin et al.* [1990] (inclination of 46°, declination of -2.2°) was assumed for the remanent magnetization direction. Plate 2d illustrates the results of the R-T-P analysis along the East Coast margin, showing that the peak of the ECMA has been shifted landward relative to the total field anomalies shown in Plate 1. Figures 3c and 4c illustrate this landward shift of the R-T-P anomaly along the EDGE-801 and BA-6 seismic lines, respectively. In both cases, the peak of the R-T-P anomaly aligns well with the sequence of seaward dipping reflectors identified from the seismic lines and the peak in the isostatic gravity anomaly calculated in this study.

The landward shift of the peak in the R-T-P anomaly relative to that of the total field magnetic anomaly is also observed in the simple forward block model shown in Figure 6. Our model illustrates the much more symmetrical shape of the R-T-P anomaly relative to the total field anomaly over the highly magnetized block representing the seaward dipping reflector sequence. Yet even in this simple case the R-T-P anomaly is not perfectly symmetric. This is due to the fact that when performing the reduction-to-the-pole calculation, it is necessary to assume a single magnetization vector. However, in our model the induced and remanent magnetization directions are slightly different. Thus even in this simple model it is impossible to remove all of the skewness in the total field magnetic anomaly. We stress this caveat when interpreting the R-T-P anomaly illustrated in Plate 2d. Nevertheless, we believe that because the current and Jurassic magnetic poles are relatively similar, reduction to the pole is an effective method for removing much of the skewness in the total field magnetic anomalies.

4.3. Peaks in R-T-P Magnetic and Isostatic Gravity Anomalies

The isostatic gravity anomaly shows a corridor of positive values running parallel to the East Coast margin (Plate 2c). Along most of the margin, the peak of the isostatic gravity anomaly is located 50–100 km landward of the peak of the total field magnetic anomaly but located close to the peak of the R-T-P anomaly. Figure 9 illustrates the spatial relationship between the peak of the isostatic gravity anomaly and the ECMA after the reduction-to-the-pole correction has been performed. To eliminate short-wavelength signals from the isostatic gravity anomaly, which are unlikely to reflect variations in deep crustal structure, we filtered the isostatic anomaly using a cosine cutoff taper to remove wavelengths <50–100 km. Along most of the margin the peaks of both fields are highly correlated. Such a close spatial relationship between the peaks of the R-T-P magnetic and the isostatic gravity anomalies is consistent with a model in which highly magnetized extrusive rocks in the upper crust generate the observed peak in the R-T-P magnetic anomaly, while the corresponding peak in the isostatic gravity anomaly is caused by the integrated density effects of the high seismic velocity lower crust and the seaward dipping reflector sequence in the upper crust.

South of 35°N the isostatic gravity high appears to lie between a double peak in the R-T-P anomaly. This double peak in the R-T-P anomaly may be caused by the falloff in magnetic anomaly toward the center of a magnetic source block, with the two peaks marking the horizontal extent of the magnetized block. This effect can be seen in Figure 6, where the R-T-P anomalies are calculated to be slightly higher at the edges of the magnetized block than at the center. The development of the double peak in the R-T-P anomaly should be more pronounced if the source body has sharp vertical boundaries, while bodies that taper toward the ends will produce a single R-T-P high located over the center of the magnetized body. (See *Talwani et al.* [1995] for the magnetic anomalies produced by a number of possible geometries for the seaward dipping reflector sequence.)

Between 35°N and the sharp change in trend of the margin around 39.5°N, the peak in both the R-T-P and isostatic anomalies are wider and extend landward, potentially indicating a larger source body in this region. Another interesting feature of this section of the margin is that between 39°N and 39.5°N the isostatic gravity high is located seaward of the peak in the R-T-P anomaly. One potential explanation for this shift in the isostatic gravity high is the high density carbonate reef observed in the LASE seismic line, which lies directly below the peak in the isostatic gravity anomaly (Figures 5a and 5b). This carbonate reef might also explain the wider nature of the isostatic gravity anomaly in this area, with the high landward anomalies

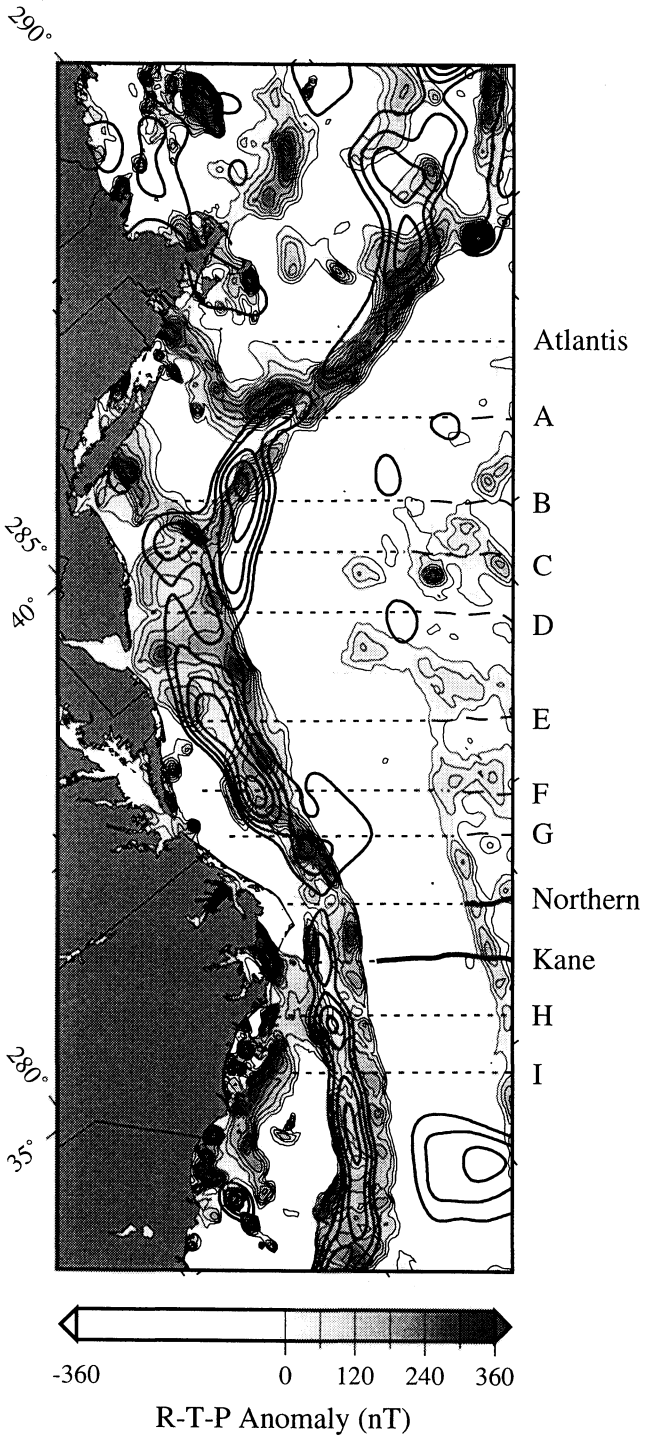

Figure 9. Comparison of R-T-P magnetic and isostatic gravity anomalies. Thin shaded contours illustrate R-T-P magnetic anomaly >0 nT with a contour interval of 60 nT. Thick contour lines without shading show filtered isostatic gravity anomaly greater than 0 mGal with a contour interval of 10 mGal. Isostatic anomalies have been low-pass filtered using a cosine cutoff taper to remove wavelengths <50–100 km. Note the strong correlation between the peak of the R-T-P anomaly and the isostatic gravity high along much of the East Coast margin. Offset zone names and locations are the same as in Plate 1.

related to the underplated material and the high seaward anomalies related to the carbonate reef.

North of 39.5°N the peak of the two fields align closely again. The magnitude of the R-T-P anomaly in this region is significantly greater than elsewhere along the margin; however, unlike the sections of the margin farther south, no double peak is observed here. In contrast, the isostatic gravity anomaly north of 39.5°N is subdued relative to the isostatic anomalies farther south. One possible interpretation of this contrast in the strength of the R-T-P and isostatic anomalies is that while the volume and width of the underplated material may be smaller north of 39.5°N, the R-T-P anomaly remains high due to the shallowing of the basement. This explanation would also account for both the small isostatic anomalies and the lack of a double peak in the R-T-P anomaly due to a decrease in width of the seaward dipping reflector sequence.

4.4. Conjugate West African Margin

In order to better understand the implications of the segmentation pattern observed along the U.S. East Coast margin, we also calculated isostatic gravity anomalies for the conjugate West African margin. Because sediment thickness data are not available for this region, the isostatic gravity anomaly was calculated by simply subtracting from free-air gravity the effects of a water-crust ($\Delta\rho$ = 1700 kg/m^3) and crust-mantle ($\Delta\rho$ = 600 kg/m^3) interface. The free-air gravity for the conjugate margin was extracted from the *Sandwell and Smith* [1997] satellite gravity map and the bathymetry was taken from ETOPO5. The depth to the crust-mantle interface was calculated from the ETOPO5 bathymetry assuming local Airy isostasy. The residual isostatic gravity anomaly for the West African margin is shown in Figure 10a. Similar to the isostatic anomaly shown in Figure 9, we have filtered the anomaly along the West African margin using a cosine cutoff taper to remove wavelengths <50–100 km. Note the strong similarity between the pattern of isostatic anomaly along the West African margin and that along the U.S. East Coast.

5. Along-Margin Segmentation and Implications

Profiles of the peak in the R-T-P magnetic and isostatic gravity anomalies along the U.S. East Coast margin show both anomalies to be strongly segmented at various wavelengths (Figures 11a and 11c). To facilitate discussion in this paper, we call anomalies with spatial wavelengths <50 km very short-wavelength features, those between 50 and 250 km short-wavelength features, and those between 250 and 500 km intermediate-wavelength features. Spectral analyses of the along-margin profiles reveal that the isostatic gravity anomaly has two distinct spectral peaks (Figure 11d) at relatively short (100–150 km) and intermediate wavelengths (300–500 km), while most of the signal power in the R-T-P ECMA corresponds to only the short wavelengths (100–120 km) (Figure 11b). Since the GSC magnetic field data were filtered to remove wavelengths >400 km [*Verhoef et al.*, 1996], the lack of a spectral peak at the intermediate wavelengths in the R-T-P magnetic anomaly may be partially an artifact of the initial data processing. The short-wavelength segmentation in the isostatic gravity anomaly is of smaller amplitude (15–30 mGal) than the intermediate-wavelength segmentation (40–60 mGal).

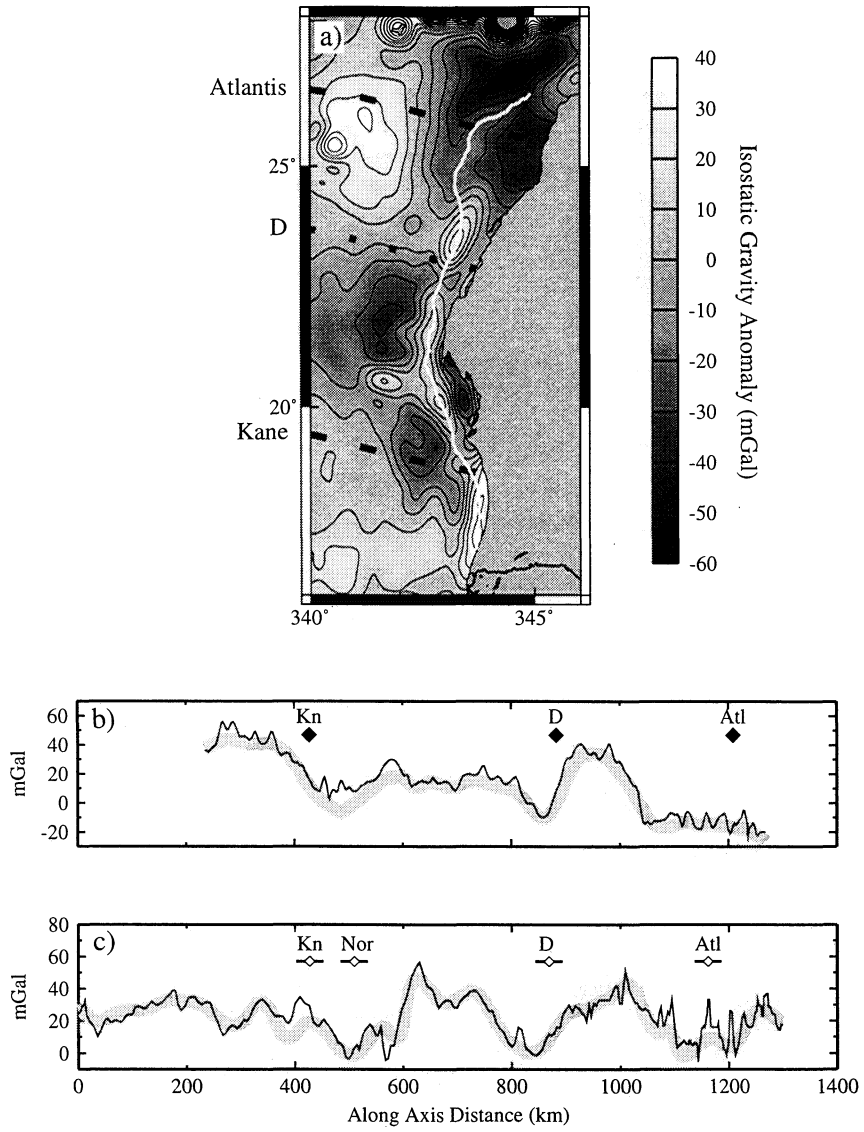

Figure 10. (a) Isostatic gravity anomaly along the West African margin conjugate to the U.S. East Coast margin, calculated by subtracting from the free-air gravity the effects of the water-crust ($\Delta\rho$ = 1700 kg/m^3) and crust-mantle ($\Delta\rho$ = 600 kg/m^3) interfaces. Isostatic anomalies have been low-pass filtered using a cosine cutoff taper to remove wavelengths <50–100 km. Dashed lines show the location of the Kane and Atlantis fracture zones projected from the Mid-Atlantic Ridge using the flow lines of *Klitgord and Schouten* [1986]; dotted line represents location of the D offset zone. Thin white line illustrates the location of profile in Figure 10b. (b) Variations in the peak of the isostatic gravity anomaly along the West African margin. Locations of Kane (Kn), Atlantis (Atl), and D offset zones are marked with solid diamonds (no estimates of uncertainty were made). (c) Variations in the peak of the isostatic gravity anomaly along the U.S. East Coast margin. Notice the similar 300–500 km wavelength variations in the isostatic gravity anomalies along both margins, with the Kane, Atlantis, Northern (Nor), and D offset zones located in the isostatic gravity lows.

5.1. Comparison to the Present-Day MAR Axis Segmentation

Crustal magnetization [*Sempéré et al.*, 1993; *Pockalny et al.*, 1995] and mantle Bouguer anomalies (MBA) [*Escartín and Lin*, 1998; *Thibaud et al.*, 1998] are also observed to vary along the present-day MAR axis (Figures 11e and 11g). Similar to the power spectra from the along-margin R-T-P magnetic and isostatic gravity anomalies (Figures 11b and 11d), the crustal magnetization of the MAR axis shows a spectral peak around a wavelength of 100–120 km (Figure 11f). The MBA of the MAR axis also shows a short-wavelength spectral peak (Figure 11h) but at a slightly longer wavelength (~150 km). The reason for the difference between the short-wavelength peak in the MBA and other three anomalies is unclear. However, it is possible that smaller offsets at the modern MAR do not provide enough variation in crustal thickness to produce a significant MBA low, thus biasing the spectral peak in the MBA toward longer wavelengths.

The along-axis magnetization and MBA show an additional spectral peak at very short wavelength of around 40–50 km, corresponding to the observed 20–80 km along-axis length of individual spreading segments bounded primarily by nontransform offsets at the MAR axis between the Kane and Atlantis fracture zones [*Sempéré et al.,* 1993]. Notice that the peak in the MBA is at a slightly longer wavelength (~50 km) than the spectral peak in the crustal magnetization (~40 km). This discrepancy may be caused by the fact that the MBA is generated by variations in Moho depth at the base of the oceanic crust, while the variations in magnetization are generated within the extrusive layer in the top 1 km of the crust. The lack of this very short-wavelength spectral peak in the along-margin R-T-P magnetic and isostatic gravity

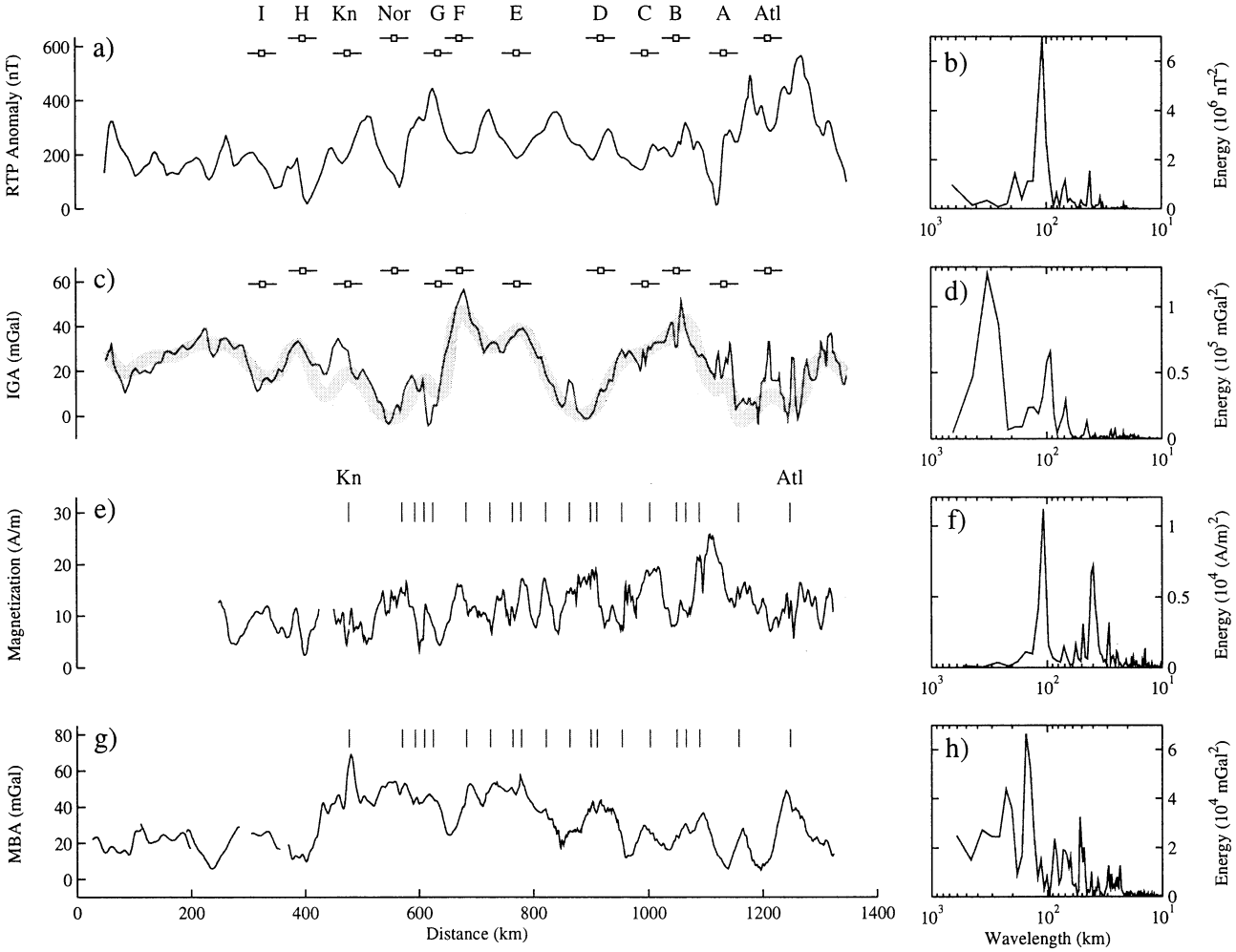

Figure 11. Comparison of variations in R-T-P magnetic and isostatic gravity anomalies along the East Coast margin to along-axis changes in crustal magnetization and mantle Bouguer anomaly (MBA) at the present-day Mid-Atlantic ridge (MAR). (a) R-T-P magnetic anomaly along the peak of the ECMA. Open squares represent the locations where the offset zones enter the margin, with bars illustrating ±25 km zones of estimated uncertainty. Along-margin distance was calculated by projecting the profile in the average flow line direction and then taking the distance perpendicular to the flow lines as the standard distance. (b) Variance conserving power spectrum for the along-margin R-T-P magnetic anomaly. (c, d) Along-margin variations in the peak of the isostatic gravity anomaly with corresponding power spectrum. The thick shaded line illustrates the filtered isostatic gravity anomaly using a cosine cutoff taper to remove wavelengths <50-100 km. (e, f) Along-axis crustal magnetization at the present-day MAR and corresponding power spectrum. Thin vertical lines represent the location of Kane and Atlantis transform faults (Kn and Atl) and numerous nontransform offsets [*Escartín and Lin* , 1998]. Data south of the Kane fracture zone are taken from *Pockalny et al.* [1995], while the data north of Kane are from *Sempéré et al.* [1993]. The crustal magnetization was calculated by downward continuation of residual magnetic anomalies assuming a 0.5-km thick magnetic source layer in the upper crust [*Sempéré et al.,* 1993; *Pockalny et al.*, 1995]. (g, h) Along-axis MBA and corresponding power spectrum. Data south of the Kane fracture zone are taken from *Thibaud et al.* [1998], while data north of Kane are from *Escartín and Lin* [1998]. Note that all four data sets show a characteristic segmentation wavelength of 100–150 km. However, only the along-margin isostatic gravity anomaly and the along-axis MBA gravity show significant spectral power at wavelengths >200 km.

anomalies may be related to the fact that the margin potential field data are highly attenuated from the source crust, typically buried beneath 5–12 km of sediments. Similar to the along-margin R-T-P magnetic anomaly, no significant power is seen in the crustal magnetization along the present-day MAR axis at wavelengths >200 km. However, the along-axis MBA profile does show signal power at the intermediate wavelengths, although it does not develop a distinct spectral peak between 300 and 500 km as in the along-margin profile of the isostatic gravity anomaly.

5.2. Relation to the Incipient Atlantic Offset Zones

The Kane and Atlantis fracture zones are the largest and most stable offsets along the section of the present-day MAR that corresponds to the East Coast margin (Figure 1). The traces of the Kane and Atlantis fracture zones intersect both the U.S. East Coast margin and the conjugate West African margin near lows in the intermediate-wavelength (300–500 km) isostatic gravity anomaly (Figures 10 and 11), although at both margins the Northern offset zone is located slightly closer to the southern isostatic gravity low than the Kane fracture zone. No other major fracture zone is observed at the present-day MAR between Kane and Atlantis (Figure 1), as would be predicted from the additional intermediate-wavelength gravity low located near offset zone D (see Figures 9 and 10).

Correlating the short-wavelength (100–150 km) segmentation in the R-T-P magnetic and isostatic gravity anomalies with the incipient locations of the hypothesized offset zones along the U.S. East Coast is much more difficult to accomplish because the spatial uncertainties in the offset zone identification are almost as large as the spatial scales of the short-wavelength along-margin anomalies. Nevertheless, several of the incipient offset zones (e.g., Atlantis, A, C, D, G, Northern, Kane, H, and I) appear to correlate with lows in both the R-T-P magnetic and isostatic gravity anomalies at the short wavelengths (100–150 km) (Figure 9).

5.3. Correlation With Across-Margin Isostatic Gravity Anomalies

Along-margin segmentation in the isostatic gravity anomaly at the intermediate wavelengths (300–500 km) also appears to be associated with the across-margin variations in the isostatic gravity anomaly. Figure 12a shows 20 across-margin profiles taken at the individual short-wavelength (100–150 km) peaks and troughs of the isostatic gravity anomaly along the margin (see Figure 12b for profile locations). In regions where the intermediate-wavelength (300–500 km) along-margin isostatic anomaly is generally high, the across-margin profiles are often characterized by a prominent peak and an adjacent low in the anomaly (i.e., in profiles 1-4, 8-10, 12-16, 18-20). This occurs regardless of whether the across-axis profile is taken at a short-wavelength (100-150 km) peak or trough in the along-margin anomaly. Conversely, in regions located within lows of the intermediate-wavelength (300–500 km) isostatic gravity anomaly, the across-margin profiles are relatively flat without a significant high-low couple (i.e., in profiles 5–7, 11, and 17). This relationship is further illustrated in Figure 12c, which shows a positive correlation between the peak value of the across-margin isostatic gravity anomaly and the mean across-margin gradients. The mean gradients were calculated by averaging the absolute value of point-to-point gradients in a 200 km spatial window around the peak value of the isostatic gravity anomaly. This relationship is significant because it shows that the isostatic gravity anomaly has a relatively uniform base value of 0 mGal, but in certain locations varies above this value, potentially reflecting enhanced underplating in these regions. We again note that profiles 5–7 are located near the incipient location of the Kane FZ, profile 17 is near the incipient location of the Atlantis FZ, and profile 11 is near the incipient location of the D offset zone.

5.4. Kane and Atlantis Fracture Zones as Boundaries of Tectonic Corridors?

The 300–500 km segmentation in the along-margin isostatic gravity anomaly is similar in wavelength to the tectonic corridors of the lithosphere seen by *Kane and Hayes* [1992] in the South Atlantic. *Kane and Hayes* [1992] observed tectonic corridors persisting for tens of millions of years, which exhibit large, along-ridge-axis variations in subsidence rate, zero-age seafloor depth, geoid rate as measured by geoid height decrease with age, and geochemical anomalies on length scales of 500–1000 km. These tectonic corridors are often bounded by major fracture zones. It has been suggested that these corridors are caused by changes in mantle temperature along and across the axis of a mid-ocean ridge and may have been present from the time of initial rifting and ridge formation [*Kane and Hayes*, 1994]. Such a deep mantle anomaly is not expected to have a direct effect on crustal magnetization, which has its source at depths above the Curie temperature, but would be expected to produce significant variations in isostatic gravity along the margin.

Our new observation of the clear correlation of the Kane and the Atlantis FZs with the intermediate-wavelength (300–500 km) isostatic gravity lows supports a hypothesis that the Kane and Atlantis FZs might be the boundaries of a tectonic corridor in the North Atlantic, similar to those observed by *Kane and Hayes* [1992, 1994] in the South Atlantic. One important implication of the tectonic corridor concept is that it predicts the boundaries of the corridor (such as the Kane and Atlantis FZs) to be much more stable and prominent in comparison to offsets occurring within the corridor interior (such as the numerous nontransform offsets observed along the present-day MAR axis between the Kane and Atlantis FZs). Another implication is that the intermediate-wavelength isostatic gravity anomaly might be a good indicator of tectonic corridors globally. These hypotheses can be tested through future investigations of other continental margins using multiple investigative approaches including the isostatic gravity analysis.

The direct cause of the observed isostatic gravity anomalies along the U.S. East Coast margin may be a combination of along-margin variations in both the amount of thickened igneous crust and the strength of the lithosphere. If igneous crustal accretion along a volcanic margin is focused toward discrete centers similar to that of an active slow spreading center, we would expect crustal underplating to be least near offset zones and greatest at the segment centers of a margin. Furthermore, it is possible that the intermediate-wavelength variations in isostatic gravity anomalies reflect the characteristic size of mantle upwelling cells during continental rifting.

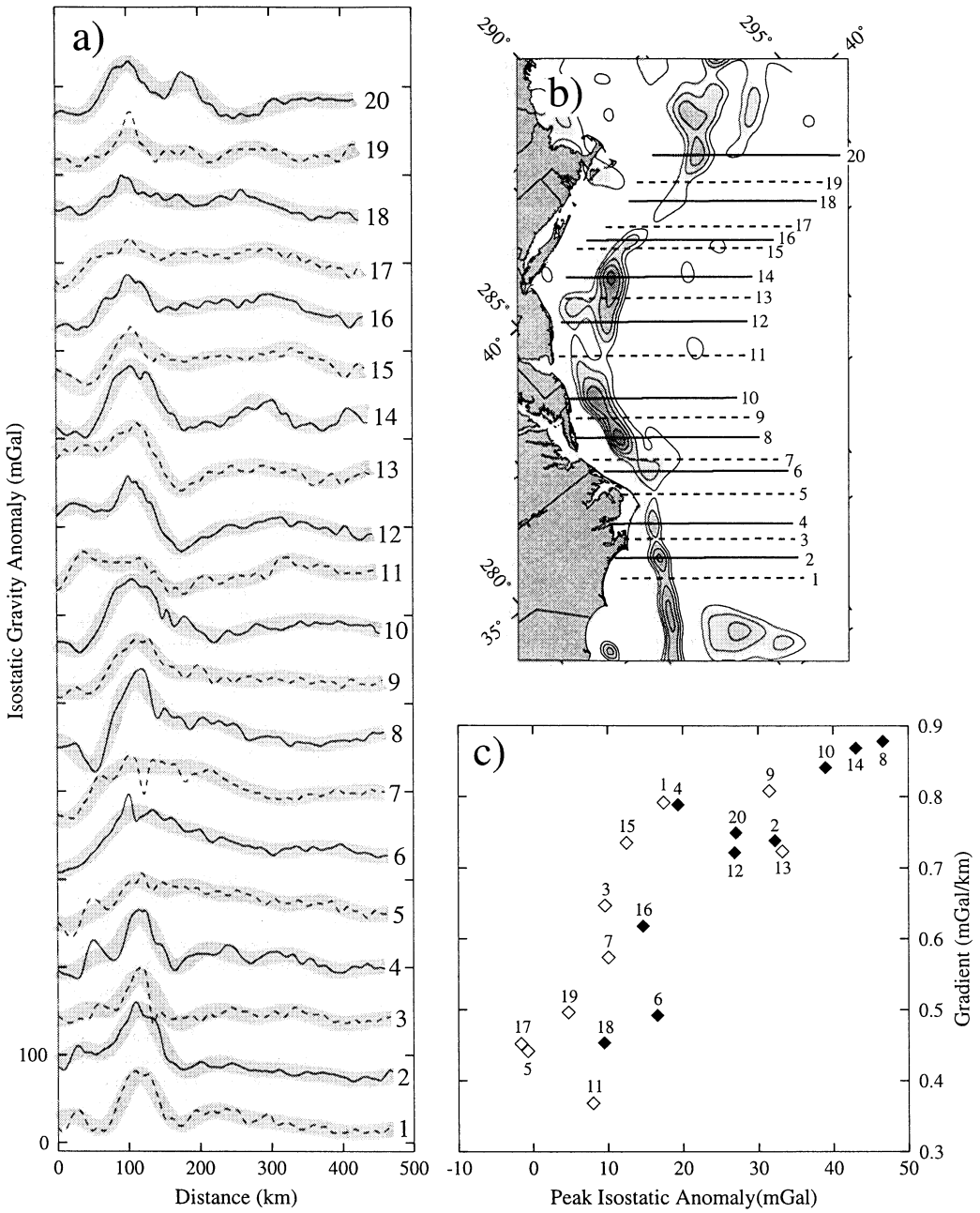

Figure 12. (a) Across-margin profiles showing variations in the isostatic gravity anomaly. Solid lines represent profiles taken through 100-150 km wavelength peaks in the isostatic gravity anomaly, while dashed lines show profiles taken through 100–150 km wavelength isostatic lows. Thick shaded lines represent the filtered isostatic anomaly calculated using a cosine cutoff taper to remove wavelengths <50–100 km. (b) Location of profiles shown in Figure 12a. Shaded contours illustrate filtered isostatic gravity anomalies greater than 0 mGal with a contour interval of 10 mGal. (c) Mean absolute gradient in across-margin anomaly versus the peak value of the isostatic gravity anomaly. The mean absolute gradient was calculated along an across-margin profile in a 200 km window around the peak value of the isostatic anomaly. Solid symbols represent across-margin profiles taken through 100–150 km wavelength isostatic highs, while open symbols represent across-margin profiles taken through isostatic lows. Note the positive relationship between the mean absolute across-margin gradient and the peak of the isostatic anomaly, indicating that as the peak of the isostatic anomaly decreases, the overall across-margin variation becomes smaller.

In addition, we hypothesize that at incipient oceanic offset zones, especially near the boundaries of tectonic corridors, the oceanic lithosphere is relatively weak and thus incapable of supporting large tectonic loads. This results in smaller values of along- and across-margin isostatic gravity anomalies, as observed near the incipient locations of the Kane and Atlantis fracture zones. *Sawyer* [1985] and *Dunbar and Sawyer* [1989] showed that preexisting weaknesses in the

structure of the U.S. East Coast may have controlled the early stages of extension along the margin. These studies concluded that seafloor spreading will tend to be focused in preexisting weak zones, leading to smaller amounts of extension in these areas relative to regions of higher initial strength. The Kane, Atlantis, and D offset zones all fall into regions of low total extension as identified by *Dunbar and Sawyer* [1989] and thus can be hypothesized to represent initial weaknesses in the U.S East Coast margin. Together with the possible variable underplating mechanism, such changes in lithospheric strength could lead to even greater along- and across-margin variations in isostatic gravity anomalies.

Changes in lithospheric strength have also been observed along other rifted continental margins. For example, by analyzing changes in the structure of the continental edge effect, *Watts and Marr* [1995] found lithospheric strength to vary on length scales of several hundred kilometers along the African margin. *Watts and Marr* [1995] correlated these variations to the location of hot spot traces, suggesting that the incidence of a hot spot on the base of the lithosphere may be capable of decreasing its effective elastic thickness. More recent work by *Watts and Stewart* [1998] found a 350–400 km weak zone to exist along the Gabon margin offshore of West Africa, suggesting that similar scale strong versus weak segmentation may be a characteristic of many rifted continental margins.

At present, however, the relative importance of the variable underplating versus variable lithospheric strength is poorly known. Recent seismic experiments along active spreading centers have played a key role in determining the relative importance of the variations in crustal thickness/density versus upper mantle structure in producing the 'bull's-eye' MBA patterns observed along the MAR [*Tolstoy et al.*, 1993; *Canales et al.*, 2000; *Hooft et al.*, 2000]. To date, most high-quality seismic experiments at volcanic margins have been carried out only in across-margin lines. The results of this study suggest a strong need for well-designed future seismic experiments to be conducted along the margins.

6. Conclusions

In this study we examine variations in the magnetic field and the isostatic gravity anomalies along the U.S. East Coast margin. We observe a corridor of high isostatic gravity anomaly running along the margin that corresponds closely to the location of the ECMA after reduction to the pole of the total field magnetic anomaly. Both of these anomalies situate close to the maximum thickness of high velocity igneous crust determined by previous seismic studies. Spectral analysis shows the R-T-P ECMA is segmented on length scales of 100–120 km, while the isostatic gravity anomaly is found to exhibit segmentation in two distinct wave bands: 100–150 km and 300–500 km. We find the 300–500 km segmentation in the isostatic gravity anomaly to have a larger amplitude (40–60 mGal) than the 100–150 km wavelength (15–30 mGal) and to coincide with an overall change in the character of the across-margin isostatic gravity anomalies.

The observed segmentation in gravity and magnetic anomalies at the U.S. East Coast margin has important implications for the formation of continental margins and the origin of segmentation at mature mid-ocean ridges. The short-wavelength (100–150 km) along-margin magnetic and isostatic gravity anomalies are similar in wavelength to the segmentation in magnetization and mantle Bouguer anomaly observed along the present-day MAR axis. Moreover, many of the short-wavelength magnetic and isostatic gravity lows correlate well to the location of early traces of identifiable Atlantic offsets. While this correlation is not one to one, such a relationship would not necessarily be expected due to the along-axis migration of nontransform offsets with time and the thick sedimentary basins attenuating the crustal gravity signal near the margin.

The 300–500 km segmentation in the along-margin isostatic gravity anomaly is similar in scale to the intermediate-wavelength tectonic segmentation observed in the South Atlantic [*Kane and Hayes*, 1992], for which a mantle source has been proposed. The intermediate-wavelength (300–500 km) isostatic gravity lows correspond to the early traces of the Kane and Atlantis FZs, suggesting that these two fracture zones may define a single tectonic corridor in the North Atlantic. The intermediate-wavelength segmentation is also similar to variations in lithospheric strength observed along the African margin [*Watts and Marr*, 1995; *Watts and Stewart*, 1998]. We hypothesize that the direct cause of the intermediate-wavelength isostatic gravity anomaly is along-margin variations in both the amount of the underplated igneous crust and the strength of the lithosphere, although the relative importance of these two effects remains unresolved. Our results imply that segmentation is an important feature of margin development and that segmentation at mature oceanic spreading centers may be directly linked to segmentation during continental rifting.

Acknowledgments. We are grateful to Debbie Hutchinson and Uri ten Brink for their help in supplying the USGS sediment thickness data and Brian Tucholke for his digital sediment thickness map of the North Atlantic. We would also like to thank Brian Tucholke, Hans Schouten, Maurice Tivey, Tony Watts, Steve Holbrook, Pierrick Roperch, Anne Tréhu, and an anonymous reviewer for their helpful suggestions and discussion during various phases of this work. This research was supported by National Science Foundation grant OCE-9811924, a WHOI Mellon Independent Study Award, and a National Defense Science and Engineering Graduate Fellowship (M. D. Behn). Contribution 10313 of Woods Hole Oceanographic Institution.

References

Alsop, L.E., and M. Talwani, The East Coast Magnetic Anomaly, *Science*, *226*, 1189-1191, 1984.

Austin, J.A., Jr., P.L. Stoffa, J.D. Phillips, J. Oh, D.S. Sawyer, G.M. Purdy, E. Reiter, and J. Makris, Crustal structure of the southeast Georgia embayment-Carolina Trough: Preliminary results of a composite seismic image of a continental suture(?) and a volcanic passive margin, *Geology*, *18*, 1023-1027, 1990.

Blakely, R.J., *Potential Theory in Gravity and Magnetic Applications*, 441 pp., Cambridge Univ. Press, New York, 1995.

Boutilier, R.R., and C.E. Keen, Small-scale convection and divergent plate boundaries, *J. Geophys. Res.*, *104*, 7389-7403, 1999.

Canales, J.P., R.S. Detrick, J. Lin, J.A. Collins, and D.R. Toomey, Crustal and upper mantle seismic structure beneath the rift mountains and across a nontransform offset at the Mid-Atlantic Ridge (35°N), *J. Geophys. Res.*, *105*, 2699-2719, 2000.

Cochran, J.R., and F. Martinez, Evidence from the northern Red Sea on the transition from continental to oceanic rifting, *Tectonophysics*, *153*, 25-53, 1988.

Detrick, R.S., H.D. Needham, and V. Renard, Gravity anomalies and crustal thickness variations along the Mid-Atlantic Ridge between 33°N and 40°N, *J. Geophys. Res.*, *100*, 3767-3787, 1995.

Dillon, W.P., and P. Popenoe, The Blake Plateau Basin and Carolina Trough, in *The Geology of North America*, vol. I2, *The Atlantic*

Continental Margin: U.S., edited by R.E. Sheridan and J.A. Grow, pp. 291-328, Geol. Soc. of Am., Boulder, Colo., 1988.

Dunbar, J.A., and D.S. Sawyer, How preexisting weaknesses control the style of continental breakup, *J. Geophys. Res.*, *94*, 7278-7292, 1989.

Escartín, J., and J. Lin, Tectonic modification of axial crustal structure: Evidence from spectral analysis of residual gravity and bathymetry of the Mid-Atlantic Ridge flanks, *Earth Planet. Sci. Lett.*, *154*, 279-293, 1998.

Grindlay, N.R., P.J. Fox, and K.C. Macdonald, Second-order ridge axis discontinuities in the South Atlantic: Morphology, structure, and evolution, *Mar. Geophys. Res.*, *13*, 21-49, 1991.

Hinz, K., A hypothesis on terrestrial catastrophes: Wedges of very thick oceanward dipping layers beneath passive margins, *Geol. Jahrb.*, *22*, 5-28, 1981.

Holbrook, W.S., and P.B. Kelemen, Large igneous province on the US Atlantic margin and implications for magmatism during continental breakup, *Nature*, *364*, 433-436, 1993.

Holbrook, W.S., G.M. Purdy, R.E. Sheridan, L. Glover, III, M. Talwani, J. Ewing, and D. Hutchinson, Seismic structure of the U.S. mid-Atlantic continental margin, *J. Geophys. Res.*, *99*, 17,871-17,891, 1994a.

Holbrook, W.S., E.C. Reiter, G.M. Purdy, D. Sawyer, P.L. Stoffa, J.A. Austin Jr., J. Oh, and J. Makris, Deep structure of the U.S. Atlantic continental margin, offshore South Carolina, from coincident ocean bottom and multichannel seismic data, *J. Geophys. Res.*, *99*, 9155-9178, 1994b.

Hooft, E.E.E., R.S. Detrick, D.R. Toomey, J.A., Collins, and J. Lin, Crustal thickness and structure along three contrasting spreading segments of the Mid-Atlantic Ridge, 33.5°–35°N, *J. Geophys. Res.*, *105*, 8205-8226, 2000.

Hopper, J.R., J.C. Mutter, R.L. Larson, C.Z. Mutter, and Northwest Australia Study Group, Magmatism and rift margin evolution: Evidence from northwest Australia, *Geology*, *20*, 853-857, 1992.

Horsefield, S.J., R.B. Whitmarsh, R.S. White, and J.-C. Sibuet, Crustal structure of the Goban Spur rifted continental margin, NE Atlantic, *Geophys. J. Int.*, *119*, 1-19, 1993.

Hutchinson, D.R., J.A. Grow, K.D. Klitgord, and B.A. Swift, Deep structure and evolution of the Carolina trough, in *Studies in Continental Margin Geology*, edited by J.S. Watkins and C.L. Drake, *Mem. Geol. Soc. Am.*, *34*, 129-152, 1983.

Hutchinson, D.R., C.W. Poag, A. Johnson, P. Popenoe, and C. Wright, Geophysical database of the East Coast of the United States: Southern Atlantic Margin--Stratigraphy and velocity in map grids, *U.S. Geol. Surv. Open File Rep.*, *96-55*, 1996.

Johnson, G.L., and P.R. Vogt, Mid-Atlantic Ridge from 47° to 51° North, *Geol. Soc. Am. Bull.*, *84*, 3443-3462, 1973.

Kane, K.A., and D.E. Hayes, Tectonic corridors in the South Atlantic: Evidence for long-lived mid-ocean ridge segmentation, *J. Geophys. Res.*, *97*, 17,317-17,330, 1992.

Kane, K.A., and D.E. Hayes, Long-lived mid-ocean ridge segmentation: Constraints on models, *J. Geophys. Res.*, *99*, 19,693-19,706, 1994.

Kelemen, P.B., and W.S. Holbrook, Origin of thick, high-velocity igneous crust along the U.S. East Coast margin, *J. Geophys. Res.*, *100*, 10,077-10,094, 1995.

Klitgord, K.D., and J.C. Behrendt, Basin structure of the U.S. Atlantic margin, in *Geological and Geophysical Investigations of Continental Margins*, edited by J.S. Watkins, L. Montadert, and P.W. Dickerson, *Mem. Geol. Soc. Am.*, *29*, 85-112, 1979.

Klitgord, K.D., and H. Schouten, The onset of sea-floor spreading from magnetic anomalies, in *Symposium on the Geological Development of the New York Blight*, pp. 12-13, Lamont-Doherty Geol. Obs., Palisades, N.Y., 1977.

Klitgord, K.D., and H. Schouten, Plate kinematics of the central Atlantic, in *The Geology of North America*, vol. M, *The Western North Atlantic Region*, edited by P.R. Vogt and B.E. Tucholke, pp. 351-377, Geol. Soc. of Am., Boulder, Colo., 1986.

Klitgord, K.D., D.R. Hutchinson, and H. Schouten, U.S. Atlantic continental margin; Structure and tectonic framework, in *The Geology of North America*, vol. I2, The *Atlantic Continental Margin, U.S.*, edited by R.E. Sheridan and J.A. Grow, pp. 19-55, Geol. Soc. of Am., Boulder, Colo., 1988.

Klitgord, K.D., C.W. Poag, C.M. Schneider, and L. North, Geophysical database of the East Coast of the United States: Northern Atlantic margin: Cross sections and gridded database, *U.S. Geol. Surv. Open File Rep.*, *94-637*, 1994.

Kuo, B., and D.W. Forsyth, Gravity anomalies of the ridge-transform system in the South Atlantic between 31° and 34.5°S: Upwelling centers and variations in crustal thickness, *Mar. Geophys. Res.*, *10*, 205-232, 1988.

LASE Study Group, Deep structure of the U.S. East Coast passive margin from large aperture seismic experiments (LASE), *Mar. Pet. Geol.*, *3*, 234-242, 1986.

Lin, J., and J. Phipps Morgan, The spreading rate dependence of three-dimensional mid-ocean ridge gravity structure, *Geophys. Res. Lett.*, *19*, 13-16, 1992.

Lin, J., G.M. Purdy, H. Schouten, J.-C. Sempere, and C. Zervas, Evidence from gravity data for focused magmatic accretion along the Mid-Atlantic Ridge, *Nature*, *344*, 627-632, 1990.

Magde, L.S., and D.W. Sparks, Three-dimensional mantle upwelling, melt generation, and melt migration beneath segmented slow spreading ridges, *J. Geophys. Res.*, *102*, 20,571-20,583, 1997.

McKenzie, D., Some remarks on the development of sedimentary basins, *Earth Planet. Sci. Lett.*, *40*, 25-32, 1978.

Mutter, J.C., M. Talwani, and P.L. Stoffa, Evidence for a thick oceanic crust adjacent to the Norwegian margin, *J. Geophys. Res.*, *89*, 483-502, 1984.

Mutter, J.C., W.R. Buck, and C.M. Zehnder, A model for the formation of thick basaltic sequences during the initiation of spreading, *J. Geophys. Res.*, *93*, 1031-1048, 1988.

Parker, R.L., The rapid calculation of potential anomalies, *Geophys. J. R. Astron. Soc.*, *31*, 447-455, 1972.

Parmentier, E.M., and J. Phipps Morgan, Spreading rate dependence of three-dimensional structure in oceanic spreading centres, *Nature*, *348*, 325-328, 1990.

Plouff, D., Gravity and magnetic fields of polygonal prisms and application to magnetic terrain corrections, *Geophysics*, *41*, 727-741, 1976.

Pockalny, R.A., A. Smith, and P. Gente, Spatial and temporal variability of crustal magnetization of a slowly spreading ridge: Mid-Atlantic Ridge (20° -24° N), *Mar. Geophys. Res.*, *17*, 301-320, 1995.

Roest, W.R., J.J. Dañobeitia, J. Verhoef, and B.J. Collette, Magnetic anomalies in the Canary Basin and the Mesozoic evolution of the central North Atlantic, *Mar. Geophys. Res.*, *14*, 1-24, 1992.

Sandwell, D.T., and W.H.F. Smith, Marine gravity anomaly from Geosat and ERS 1 satellite altimetry, *J. Geophys. Res.*, *102*, 10,039-10,054, 1997.

Sawyer, D.S., Total tectonic subsidence: A parameter for distinguishing crust type at the U.S. Atlantic continental margin, *J. Geophys. Res.*, *90*, 7751-7769, 1985.

Schouten, H., H.J.B. Dick, and K.D. Klitgord, Migration of mid-ocean-ridge volcanic segments, *Nature*, *326*, 835-839, 1987.

Sempéré, J.-C., J. Lin, H.S. Brown, H. Schouten, and G.M. Purdy, Segmentation and morphotectonic variations along a slow-spreading center: The Mid-Atlantic Ridge (24°00'N - 30°40'N), *Mar. Geophys. Res.*, *15*, 153-200, 1993.

Simpson, R.W., R.C. Jachens, R.J. Blakely, and R.W. Saltus, A new isostatic residual gravity map of the conterminous United States with a discussion on the significance of isostatic residual anomalies, *J. Geophys. Res.*, *91*, 8348-8372, 1986.

Talwani, M., J. Ewing, R.E. Sheridan, W.S. Holbrook, and L. Glover III, The Edge Experiment and the U.S. East Coast Magnetic Anomaly, in *Rifted Ocean-Continental Boundaries*, edited by E. Banda, M. Torne, and M. Talwani, pp. 155-181, Kluwer Acad., Norwell, Mass., 1995.

Thibaud, R., P. Gente, and M. Maia, A systematic analysis of the Mid-Atlantic Ridge morphology and gravity between 15°N and 40°N: Constraints of the thermal structure, *J. Geophys. Res.*, *103*, 24,223-24,243, 1998.

Tolstoy, M., A.J. Harding, and J.A. Orcutt, Crustal thickness on the Mid-Atlantic Ridge: Bull's-eye gravity anomalies and focused accretion, *Science*, *262*, 726-729, 1993.

Tréhu, A.M., A. Ballard, L.M. Dorman, J.F. Gettrust, K.D. Klitgord, and A. Schreiner, Structure of the lower crust beneath the Carolina Trough, U.S. Atlantic continental margin, *J. Geophys. Res.*, *94*, 10,585-10,600, 1989a.

Tréhu, A.M., K.D. Klitgord, D.S. Sawyer, and R.T. Buffler, Atlantic and Gulf of Mexico continental margins, in *Geophysical Framework of the Continental United States*, edited by L.C. Pakiser and W.D. Mooney, *Mem. Geol. Soc. Am.*, *172*, 349-382, 1989b.

Tucholke, B.E., and J. Lin, A geological model for the structure of ridge segments in slow spreading ocean crust, *J. Geophys. Res.*, *99*, 11,937-11,958, 1994.

Tucholke, B.E., and H. Schouten, Kane fracture zone, *Mar. Geophys. Res.*, *10*, 1-39, 1988.

Tucholke, B.E., R.E. Houtz, and W.J. Ludwig, Sediment thickness and depth to basement in western North Atlantic Ocean basin, *AAPG Bull.*, *66*, 1384-1395, 1982.

Tucholke, B.E., J. Lin, M.C. Kleinrock, M.A. Tivey, T.B Reed, J. Goff, and G.E. Jaroslow, Segmentation and crustal structure of the western Mid-Atlantic Ridge flank, 25°25'–27°10'N and 0-29 m.y., *J. Geophys. Res. 102*, 10,203-10,223, 1997.

Uchupi, E., J.D. Phillips, and K.E. Prada, Origin and structure of the New England Seamount Chain, *Deep Sea Res.*, *17*, 483-494, 1970.

Verhoef, J., B.J. Collette, J.J. Dañobeitia, H.A. Roeser, and W.R. Roest, Magnetic anomalies off West-Africa (20–38°N), *Mar. Geophys. Res.*, *13*, 81-103, 1991.

Verhoef, J., W.R. Roest, R. Macnab, and J. Arkani-Hamed, Magnetic anomalies of the Arctic and North Atlantic Oceans and adjacent land areas, *Geol. Surv. Can. Open File Rep.*, *3125*, 1996.

Vogt, P.R., Early events in the opening of the North Atlantic, in *Implications of Continental Drift to the Earth Sciences*, edited by D.H. Tarling and S.K. Runcorn, pp. 693-712, Academic, San Diego, Calif., 1973.

Watts, A.B., and C. Marr, Gravity anomalies and the thermal and mechanical structure of rifted continental margins, in *Rifted Ocean-Continental Boundaries*, edited by E. Banda, M. Torne, and M. Talwani, pp. 65-94, Kluwer Acad., Norwell, Mass., 1995.

Watts, A.B., and J. Stewart, Gravity anomalies and segmentation of the continental margin offshore West Africa, *Earth Planet. Sci. Lett.*, *156*, 239-252, 1998.

White, R., and D. McKenzie, Magmatism at rift zones: The generation of volcanic continental margins and flood basalts, *J. Geophys. Res.*, *94*, 7685-7729, 1989.

White, R.S., G.K. Westbrook, S.R. Fowler, G.D. Spence, P.J. Barton, M. Joppen, J. Morgan, A.N. Bowen, C. Prescott, and M.H.P. Bott, Hatton Bank (northwest UK) continental margin structure, *Geophys. J. R. Astron. Soc.*, *89*, 265-271, 1987.

Whitehead, J.A., Jr., H.J.B. Dick, and H. Schouten, A mechanism for magmatic accretion under spreading centres, *Nature*, *312*, 146-148, 1984.

Whitmarsh, R.B., et al., Drilling reveals transition from continental breakup to early magmatic crust, *Eos Trans. AGU*, *79*, 173, 180-181, 1998.

M.D. Behn, MIT-WHOI Joint Program, 77 Massachusetts Avenue, Building 54-521, Cambridge, MA 02139. (mbehn@mit.edu)

J. Lin, Department of Geology and Geophysics, Woods Hole Oceanographic Institution, Woods Hole, MA 02543. (jlin@whoi.edu)

(Received December 17, 1999; revised June 15, 2000;
accepted July 26, 2000.)